The Chiral approach of the $\Xi(1620)$ and $\Xi(1690)$ resonances in the $\Xi_c^+ \to \pi^+\pi^+\Xi^-$ decay

by

Victoria Valcarce Cadenas

Supervisors: Volodymyr Magas and Albert Feijoo

Interuniversity Master of Nuclear Physics

Final Master Thesis

Department of Quantum Physics and Astrophysics

University of Barcelona

July 2023

Abstract

We study s-wave meson-baryon interactions with strangeness $S = -2$ in a coupled-channels chiral approach incorporating not only the leading Weinberg-Tomozawa term in the Lagrangian, but also the Born terms and next-to-leading order contributions. With our model we fit the experimental data set of the nonleptonic $\Xi_c^+ \to \pi^+\pi^+\Xi^-$ weak decay from the Belle Collaboration, where the observation of the double strange baryons $\Xi(1620)$ and $\Xi(1690)$ in their decay to $\pi^+\Xi^-$ was reported. We calculate the invariant mass distribution of the $\pi^+\Xi^-$ final state, showing that our theoretical prediction is capable of explaining the experimental data by reproducing the two resonance peaks. Regarding the pole content, we are able to dynamically generate two poles not far away from the known experimental values of the $\Xi(1620)$ and $\Xi(1690)$ states. In our approach these resonances have a molecular nature, where the lowest one strongly couples to the $\pi\Xi$ channels, while the second pole couples more strongly to the $\bar{K}\Sigma$ channels.

Acknowledgments

I would like to express my sincere gratitude to my supervisors, Prof. Volodymyr Magas and Prof. Albert Feijoo, for their constant availability to help and advise me throughout the whole project. Their invaluable patience and support have been instrumental in my progress. I have had the opportunity to learn a great deal from them, and their passion for the subject has truly inspired me. I appreciate their approachability, which has made me feel like a valued member of the team, and the trust they placed in me from the very beginning of my bachelor's thesis. I am grateful that they have chosen to be my mentors once again in this new stage.

The involvement of Prof. M. Sumihama and her contribution in providing us with the experimental data from the Belle Collaboration has been essential in shaping this project.

Contents

Chapter 1

Introduction

At present, our knowledge of how fundamental particles interact and behave is framed by what is known as the Standard Model (SM). This theory has achieved a remarkable level of success, with no significant discrepancies between its theoretical predictions and experimental measurements. However, there are still many phenomena that lack a satisfactory explanation. The Large Hadron Collider (LHC), built by CERN, aims to contribute to solving the weaknesses of the SM by searching for evidence of new physics from the discovery of new subatomic particles and the study of their internal structure.

The SM holds that there are two types of elementary particles in nature depending on whether they have half-integer or integer spin: fermions and bosons, respectively. The first ones are the basic constituents of matter and interact with each other through an exchange of the so-called gauge bosons. Fermions are classified into quarks and leptons. Each group consists of six particles paired in "generations". The lightest and most stable particles constitute the first generation, while the heaviest and least stable ones belong to the second and third generations. All the stable matter in the universe is made up of particles pertaining to the first generation, since any heavier particles decay rapidly (from a few microseconds to times on the order of 10^{-24} s) into more stable ones. The strong interaction keeps quarks bound in hadrons: baryons, with three valence quarks (qqq); and mesons, with a valence pair quark-antiquark ($q\bar{q}$) [1]. The associated boson is the gluon and the field theory describing its interaction with

[1] Other exotic configurations can also exist since the discovery of the first tetraquark $X(3872)$, which is made of ($qq\bar{q}\bar{q}$), at the Belle detector in 2003 [1]; and the first pentaquark $P_c(4380)$, composed of ($qqqq\bar{q}$), at LHCb in 2015 [2].

quarks is quantum chromodynamics (QCD).

The non-Abelian nature of QCD has interesting consequences to which two properties are related: the "confinement" and the "asymptotic freedom". The first one is responsible for the fact that free quarks have never been observed, as only "white" particle states can be found in nature. Quarks have an associated quantum number called "colour", which can be red, green or blue, so the resulting quark cluster must be colourless. This phenomenon is due to the fact that the strong force acts on the colour charge of quarks, increasing with distance. So for low energies (< 1 GeV) or, equivalently, for large distances (≥ 1 fm), the coupling force is strong. In contrast, at short distances or high energies quarks exhibit asymptotic freedom, i.e., they have a quasi-free particle behaviour due to the sufficiently weak quark-gluon coupling.

Consequently, at high momentum transfers, strong interactions are described by the scattering of quarks and gluons, and perturbative methods can be applied since the strong coupling is small at short distances. Nevertheless, at lower energies –where most hadronic and nuclear processes occur– QCD is strongly coupled, and a non-perturbative analysis is needed because a power expansion of the coupling constant would diverge. In this regime, a high energy independent dynamics would be necessary, where the degrees of freedom (d.o.f.) of the Lagrangian are no longer quarks and gluons –but hadrons– in order to be able to carry out a perturbative expansion of it. Thus, one must resort to effective theories which respects the symmetries of QCD, in particular, chiral symmetry and chiral spontaneous symmetry breaking patterns.

The strong interaction is determined by a special symmetry between the colour charges of quarks, the *SU(3)* gauge group, and quarks transform under this group as *SU(3)* triplets of fermionic Dirac fields. The chiral symmetry implies the invariance of the dynamics to independent transformations of the dextrorotatory and levorotatory parts of the Dirac fields representing the quarks. This can only occur exactly if the fermion masses are zero, so the existence of an approximate chiral symmetry in QCD is only possible for flavour sectors where the quark masses are small. Henceforth, our focus will be directed towards the three light quarks *up* (u), *down* (d) and *strange* (s).

A good candidate for an effective theory is *SU(3)* Chiral Perturbation Theory (χPT), which at low energies satisfactorily describes meson-meson, meson-baryon and baryon-baryon interactions. However, it fails in the vicinity of a resonance, i.e., baryonic or mesonic excited states, since these are associated with a pole in the scattering amplitude that cannot be reproduced by a perturbative expansion. Unitarized Chiral Perturbation Theory $(U\chi PT)$, which combines chiral dynamics with unitarization techniques in coupled channels, turns out to be a very powerful solution to this problem, allowing to describe the so-called dynamically generated resonances (i.e., those appearing as a consequence of the model).

Recent experiments –such as LHCb, *BABAR*, or Belle– have made a significant and successful contribution to the field of Hadronic Physics. These experiments have provided new insights into reactions and decays of heavy hadrons, sparking a flurry of experimental and theoretical investigations. Quantum numbers of various nucleons and hyperon resonances with strangeness $S = -1$ have been successfully measured. However, the number of observed Ξ states (hyperon resonances with $S = -2$) remains notably smaller. Hence, it is crucial to explore these unusual states and their connection to the underlying baryon structure. A key aspect of understanding them is the determination of the mass of the lowest excited states. The $\Xi(1620)$ and $\Xi(1690)$ are potential candidates, but their true nature has yet to be verified. According to the Particle Data Group (PDG) [3], they are assigned a status of one and three stars, respectively. Both are identified with an isospin of $I = 1/2$, forming the $\Xi^0(uss)$ and $\Xi^-(dss)$ doublet. However, their spin and parity (J^P) remain unknown. Several theoretical and experimental studies point to a value of $J^P = 1/2^-$, supporting the fact that they are meson-baryon molecular states.

The experimental evidence for the $\Xi(1620)$ is limited. In the 1970s, weak signals were reported in the $\pi\Xi$ channel of $K^- p$ interactions [4–6]. Nonetheless, the measurements were accompanied by large statistical uncertainties. It was not until 2019 that the Belle detector, at the KEKB asymmetric-energy e^+e^- collider, collected the first observation of this hyperon in its decay to $\pi^+\Xi^-$ via the $\Xi_c^+ \to \pi^+\pi^+\Xi^-$ process (see Fig. 2a in [7]). The subsequent data analysis determined its mass and width as:

$$M = 1610.4 \pm 6.0\ (\text{stat})^{+6.1}_{-4.2}\ (\text{syst})\ \text{MeV}\ , \quad \Gamma = 59.9 \pm 4.8\ (\text{stat})^{+2.8}_{-7.1}\ (\text{syst})\ \text{MeV}\ . \quad (1.1)$$

Interestingly enough, this study revealed at the same time a structure attributed to the $\Xi(1690)^0$ state with a significant evidence at a confidence level of 4σ.

The understanding of the $\Xi(1690)$ has improved over time with various experimental observations. Historically, this state was initially discovered as a threshold enhancement in the mass spectra of neutral and negatively charged $\bar{K}\Sigma$ particles in the $K^- p \to (\bar{K}\Sigma)K\pi$ reaction [8]. Subsequently, this resonance was observed in interactions between hyperons and nucleons [9–11], as well as in decays of charm baryons [12–15]. In a recent experiment studying the $\Xi_b^- \to J/\psi K^- \Lambda$ decay by the LHCb Collaboration, the presence of the excited state $\Xi(1690)^-$ was confirmed [16], identifying its mass and width with high precision:

$$M = 1692.0 \pm 1.3\ (\text{stat})^{+1.2}_{-0.4}\ (\text{syst})\ \text{MeV}\ , \quad \Gamma = 25.9 \pm 9.5\ (\text{stat})^{+14.0}_{-13.5}\ (\text{syst})\ \text{MeV}\ . \tag{1.2}$$

On the theoretical side, the nature of the $\Xi(1620)$ and $\Xi(1690)$ states continues to be a subject of ongoing debate and controversy. There are certain indications pointing to the fact that these resonances may have a nontrivial internal structure rather than a plain qqq configuration. The unavoidable analogy between $\Xi(1620)$ and $\Lambda(1405)$[2], as its counterpart in S = -1, leads one to interpret the $\Xi(1620)$ as a molecular state arising from UχPT scheme. Expanding on this theoretical line of investigation, in Ref. [17], the authors dynamically generate the $\Xi(1620)$ resonance but with a relatively large decay width. The results of the study showed a strong coupling of the resonance to the $\pi\Xi$ and $\bar{K}\Lambda$ channels, supporting its assignment to $J^P = 1/2^-$. More recently, in Ref. [18], at the expense of reducing unnaturally one of the parameters present in the unitarization method, the $\Xi(1620)$ was pinned down to the experimental value.

Regarding the $\Xi(1690)$ state, it has been studied in terms of its branching ratios, particularly the $\Gamma_{\pi\Xi}/\Gamma_{\bar{K}\Sigma}$ one as reported in Ref. [3]. Surprisingly, despite the larger phase space that $\pi\Xi$ has compared to $\bar{K}\Sigma$, this ratio is found to be less tan 0.09. This issue was addressed in Ref. [19], where the $\Xi(1690)$ was interpreted as a $\bar{K}\Sigma$ quasibound state dynamically generated within the framework of UχPT, in good

[2] Since 2021, the molecular nature of the $\Lambda(1405)$ has been recognized and noted in the PDG.

agreement with experimental mass yet with a tiny width. The analysis revealed that the state is strongly coupled to the $\bar{K}\Sigma$ and $\eta\Xi$ channels, while exhibiting negligible couplings to the $\pi\Xi$ one. Consequently, assuming this molecular interpretation of the resonance structure, the small value of the above branching ratio is explained.

In view of the problem of the dynamic generation of these two Ξ^* states, there exists a mutual incompatibility in pinning down both masses simultaneously. In all previous theoretical works, only a contact Weinberg-Tomozawa (WT)-like term was used as interaction. Further perturbative corrections were systematically ignored since they are assumed to play a very moderate role, specially, in s-wave. In view of that, in a recent works [20,21], we challenged this assumption to see if indeed these higher order terms could help to accomodate both resonances within the experimental values.

In the $S = -1$ sector by looking at $\bar{K}N$ interaction we can found evidences of the non-negligible role of the s- and u-channels, known as direct and cross Born terms, and the tree level next-to-leading order (NLO) contribution, diagrammatically represented in Fig. 1.1. For instance, in Ref. [22], the authors pointed out that the Born contributions reach 20% of the dominant WT contribution just 65 MeV above the $\bar{K}N$ threshold. As the energy increases moderately, the combined effect between the Born and the NLO terms play a crucial role in the reproduction of the total cross section from $\bar{K}N \to \eta\Lambda, \eta\Sigma, K\Xi$ processes [23–25]. At this point, it should be recalled that the value of the η-channel thresholds are located a little bit more than 200 MeV above $\bar{K}N$ threshold. Similarly, the difference between $\bar{K}^0\Lambda$ and the $\eta\Xi^0$ threshold is around 250 MeV. Thus, in the $S = -2$ sector a similar impact of these terms can be expected in the energy regime delimited by the higher thresholds. These new pieces in the interaction kernel will enable processes that are not connected with the WT term and, consequently, the additional interplay among the channels may affect the widths and the locations of the dynamically generated states.

With all this in mind, in Ref. [20], we incorporated to the meson-baryon interaction in the neutral $S = -2$ sector, in addition to WT term, the s-,u-channel Born diagrams and the tree level NLO contribution, by adapting the BCN model (WT+Born+NLO model in Ref. [25]). And we showed that such an extended model is able to generate

dynamically both $\Xi(1620)$ and $\Xi(1690)$ states in a fair agreement with the PDG compilation. Building upon these findings, we furthered our research in Ref. [21], refining the obtained results. Given the recent evidence of the $\Xi(1620)$ and $\Xi(1690)$ states in the $\Xi_c^+ \to \pi^+\pi^+\Xi^-$ decay observed by the Belle Collaboration [7], our objective now is to broaden our investigation by applying our theoretical model in an effort to explain these experimental data. The present work will be focused into this research task.

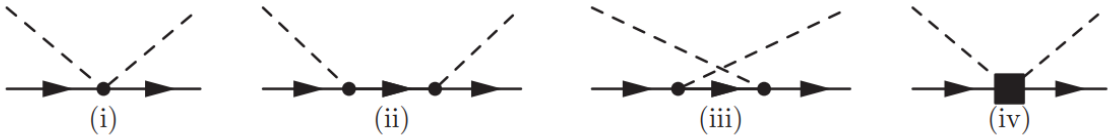

Figure 1.1: Feynman diagrams for meson-baryon interaction: WT term (i), direct (ii) and crossed (iii) Born terms, and NLO terms (iv). Solid (dashed) lines represent the fundamental octet baryons (pseudoescalar octet mesons).

Chapter 2

Chiral Unitary Approach

As already discussed in Chapter 1, quark dynamics are well described by QCD at high energies. In particular, we mentioned that as a non-Abelian gauge theory the strong coupling constant becomes large at low energies and it is not possible to treat the interactions as perturbations of a free Lagrangian. To solve this problem, we employ chiral effective field theories, which use hadrons as the d.o.f. and have Lagrangians that incorporate the main symmetries of QCD. UχPT allow us to reproduce the observed phenomenology of hadrons through a set of operators accompanied by the associated coefficients, the so-called low-energy constants (LECs). This section provides a development of the coupled channel formalism employed for describing meson-baryon scattering (for a more detailed explanation see Ref. [26]).

2.1 Lagrangian and interaction kernel

The starting point is the $SU(3)_R \times SU(3)_L$ chiral effective Lagrangian that describes the coupling of the octet of pseudoscalar mesons (π, K, η) to the octet of $1/2^+$ baryons (N, Λ, Σ, Ξ),

$$\mathcal{L}_{eff} = \mathcal{L}^{(1)}_{\phi B} + \mathcal{L}^{(2)}_{\phi B} \ , \tag{2.1}$$

which consists of an expansion in powers of momentum where the number in parentheses points to the number of powers in each term. The first term corresponds to the lowest order (LO) contributions, while the second one is the next-to-leading order

(NLO) term. Since higher orders only introduce small corrections to the main term and for each higher order contribution introduced the number of LECs rapidly grows, 2nd order higher terms have been neglected in this work.

At LO $\mathcal{O}(p)$, the most general form of the Lagrangian is given by

$$\mathcal{L}_{\phi B}^{(1)} = \langle \bar{B}(i\gamma_\mu D^\mu - M_0)B\rangle - \frac{1}{2}D\langle \bar{B}\gamma_\mu\gamma^5\{u^\mu, B\}\rangle - \frac{1}{2}F\langle \bar{B}\gamma_\mu\gamma^5[u^\mu, B]\rangle \ , \tag{2.2}$$

where the first term can provide the contact interaction of the meson-baryon, known in the literature as the Weinberg-Tomozawa (WT) term. The other terms associated to the coefficients D and F give a contribution to the s- and u-channel interactions, which are usually called direct Born (DB) term and crossed Born (CB) term, respectively.

The 3×3 unitary matrix B contains the fundamental baryon octet:

$$B = \begin{pmatrix} \frac{1}{\sqrt{2}}\Sigma^0 + \frac{1}{\sqrt{6}}\Lambda & \Sigma^+ & p \\ \Sigma^- & -\frac{1}{\sqrt{2}}\Sigma^0 + \frac{1}{\sqrt{6}}\Lambda & n \\ \Xi^- & \Xi^0 & -\frac{2}{\sqrt{6}}\Lambda \end{pmatrix} \ . \tag{2.3}$$

The incorporation of the pseudoscalar meson octet requires a more complicated prescription, $u^\mu = iu^\dagger\partial^\mu U u^\dagger$, to preserve the chiral symmetry. The pseudoscalar fields are collected in a 3×3 unitary matrix,

$$\phi = \begin{pmatrix} \frac{1}{\sqrt{2}}\pi^0 + \frac{1}{\sqrt{6}}\eta & \pi^+ & K^+ \\ \pi^- & -\frac{1}{\sqrt{2}}\pi^0 + \frac{1}{\sqrt{6}}\eta & K^0 \\ K^- & \bar{K}^0 & -\frac{2}{\sqrt{6}}\eta \end{pmatrix} \ , \tag{2.4}$$

which enters via

$$u^2(\phi) = U(\phi) = \exp\left(i\frac{\phi}{f}\right) = \mathbb{1} + \frac{i\phi}{\sqrt{2}f} - \frac{\phi^2}{4f^2} + ... \ , \tag{2.5}$$

where f is the meson decay constant in the chiral limit.

In Eq. (2.2), the braket $\langle ... \rangle$ stands for the trace of its argument and M_0 is the common baryon octet mass in the chiral limit. The LECs D and F are the $SU(3)$ axial vector constants [1] subject to the constraint $g_A = D + F = 1.26 \pm 0.05$; which arises from the determination of neutron and hyperon β decays [27]. Another important definition is the covariant derivative D^μ acting on B, being the chiral connection:

$$D^\mu B = \partial^\mu B + [\Gamma^\mu, B] \quad \text{where} \quad \Gamma^\mu = \frac{1}{2}\left[u^\dagger, \partial^\mu u\right] \ . \tag{2.6}$$

Developing the WT term of the Lagrangian in Eq. (2.2) in a non-relativistic limit

$$\mathcal{L}_{\phi B}^{WT} = \langle \bar{B} i\gamma_\mu \left[(\phi\partial^\mu\phi - \partial^\mu\phi\phi)B - B(\phi\partial^\mu\phi - \partial^\mu\phi\phi)\right]\rangle \ , \tag{2.7}$$

one can derive the meson-baryon interaction kernel associated (see representation (i) in Fig. 1.1), which reads:

$$V_{ij}^{WT} = -C_{ij}\frac{1}{4f^2}\mathcal{N}_i\mathcal{N}_j(2\sqrt{s} - M_i - M_j) \ , \tag{2.8}$$

where the sub-indexes i, j denote the incoming and outgoing meson-baryon channel. $N_i = \sqrt{(M_i + E_i)/2M_i}$ is the normalization factor with $E_i = (s + M_i^2 - m_i^2)/(2\sqrt{s})$ being the energy of the baryon. M_i and m_i are, respectively, the physical masses of the baryon and the meson in channel i; and $\sqrt{s}$ is the total center-of-mass (CM) energy of the system.

As it is seen, the WT term depends only on one parameter - the pion decay constant f, which is well known experimentally, $f_\pi = 93$ MeV (pp. 670, 687 in Ref. [28]). However, in UχPT calculations this parameter is usually ranging from $f = 1.15 f_\pi$ to $f = 1.20 f_\pi$, meaning to be a sort of average over the decay constants of the mesons involved in the various coupled channels [25]. The indices (i, j) cover all the initial and final channels which, in the case of strangeness $S = -2$ and charge $Q = 0$

[1] Usually, but not necessarily, fixed at the values $D = 0.8$ and $F = 0.46$.

explored here, amount to six: $\pi^+\Xi^-$, $\pi^0\Xi^0$, $\bar{K}^0\Lambda$, $K^-\Sigma^+$, $\bar{K}^0\Sigma^0$, $\eta\Xi^0$.

The constants C_{ij} are determined by $SU(3)$ Clebsch-Gordan coefficients. We obtained them (see Table 2.1) by introducing the meson and baryon fields in their matrix form and computing them in the Lagrangian using Mathematica program. In the case of baryonic fields, the incoming baryons are introduced as B, while the outgoing ones are included in $\bar{B} = B^\dagger\gamma^0$. Conversely, the degrees of freedom for mesons, both those present in the initial state and those resulting from the interaction, are collected by ϕ. Therefore, the outgoing mesons are included as antiparticles in the initial state because the field that encompasses them refers to destruction.

C_{ij}	$\pi^+\Xi^-$	$\pi^0\Xi^0$	$\bar{K}^0\Lambda$	$K^-\Sigma^+$	$\bar{K}^0\Sigma^0$	$\eta\Xi^0$
$\pi^+\Xi^-$	1	$-\sqrt{2}$	$-\sqrt{3/2}$	0	$-\frac{1}{\sqrt{2}}$	0
$\pi^0\Xi^0$		0	$\sqrt{3}/2$	$-1/\sqrt{2}$	$-1/2$	0
$\bar{K}^0\Lambda$			0	0	0	$-3/2$
$K^-\Sigma^+$				1	$-\sqrt{2}$	$-\sqrt{3/2}$
$\bar{K}^0\Sigma^0$					0	$\sqrt{3}/2$
$\eta\Xi^0$						0

Table 2.1: C_{ij} coefficients in the WT contact potential of the pseudoescalar meson and the fundamental baryon octet with strangeness $S = -2$ and charge $Q = 0$. The coefficients are symmetric, $C_{ji} = C_{ij}$.

Next in the χPT hierarchy are the Born terms from Eq. (2.2). Developing the expression, one gets:

$$\mathcal{L}_{\phi B}^{Born} = -\frac{1}{\sqrt{2}f}(D\langle\bar{B}\gamma_5\gamma^\mu(\partial_\mu\phi B + B\partial_\mu\phi)\rangle + F\langle\bar{B}\gamma_5\gamma^\mu(\partial_\mu\phi B - B\partial_\mu\phi)\rangle) \quad . \tag{2.9}$$

Following Feynman's rules, we constructed the DB and CB diagrams to obtain the interaction kernel. Considering the s-wave projection and the non relativistic assumption, their expressions read as

$$V_{ij}^{DB} = -\sum_{k=1}^{8} \frac{C_{\bar{i}i,k}^{Born} C_{\bar{j}j,k}^{Born}}{12f^2} \mathcal{N}_i \mathcal{N}_j \frac{(\sqrt{s} - M_i)(\sqrt{s} - M_k)(\sqrt{s} - M_j)}{s - M_k^2} \tag{2.10}$$

and

$$\begin{aligned} V_{ij}^{CB} = \sum_{k=1}^{8} \frac{C_{\bar{j}k,i}^{Born} C_{\bar{i}k,j}^{Born}}{12f^2} \mathcal{N}_i \mathcal{N}_j \Bigg[& \sqrt{s} + M_k - \frac{(M_i + M_k)(M_j + M_k)}{2(M_i + E_i)(M_j + E_j)} (\sqrt{s} - M_k + M_i + M_j) \\ & + \frac{(M_i + M_k)(M_j + M_k)}{4 q_i q_j} \Bigg\{ \sqrt{s} + M_k - M_i - M_j - \frac{s + M_k^2 - m_i^2 - m_j^2 - 2E_i E_j}{2(M_i + E_i)(M_j + E_j)} \\ & \cdot (\sqrt{s} - M_k + M_i + M_j) \Bigg\} \ln \left(\frac{s + M_k^2 - m_i^2 - m_j^2 - 2E_i E_j - 2q_i q_j}{s + M_k^2 - m_i^2 - m_j^2 - 2E_i E_j + 2q_i q_j} \right) \Bigg] \ , \end{aligned} \tag{2.11}$$

with

$$q_i = \frac{\sqrt{(s - (M_i + m_i)^2)(s - (M_i - m_i)^2)}}{2\sqrt{s}} \tag{2.12}$$

being the CM three-momentum. We see in Fig. 1.1 (terms (ii) and (iii)) that the reaction goes $\phi_i B_i \to B_k \to \phi_j B_j$, where B_k is the intermediate baryon. The sum over k extends to all possible baryons of the octet. However, as B_k needs to preserve the same quantum numbers as the incoming and outgoing meson-baryon pair (i.e., $S = -2$ and $Q = 0$) there is just one possibility for the DB term within the field basis considered, the Ξ^0 particle. The Born coefficients, which include the constants D and F, integrate the total effective coupling for each transition $\bar{i}i \to \bar{j}j$ for each baryon k involved in the interaction. They are given by the product of the coupling constants, $C_{\bar{i}i,k}^{Born} C_{\bar{j}j,k}^{Born}$, of each vertex of the Feynmann diagram, where their compilation are:

$$C_{K^- p,\Lambda}^{(Born)} = C_{\bar{K}^0 n,\Lambda}^{(Born)} = C_{\eta\Xi^-,\Xi^-}^{(Born)} = C_{\eta\Xi^0,\Xi^0}^{(Born)} = -D - 3F \ ,$$

$$\sqrt{2} C_{K^- p,\Sigma^0}^{(Born)} = -\sqrt{2} C_{\bar{K}^0 n,\Sigma^0}^{(Born)} = C_{\pi^+\Xi^-,\Xi^0}^{(Born)} = C_{\pi^0\Xi^-,\Xi^-}^{(Born)} = -\sqrt{2} C_{\pi^0\Xi^0,\Xi^0}^{(Born)} = \sqrt{6}(D - F) \ ,$$

$$C_{\pi^0\Sigma^0,\Lambda}^{(Born)} = C_{\pi^-\Sigma^+,\Lambda}^{(Born)} = C_{\eta\Sigma^+,\Sigma^+}^{(Born)} = C_{\eta\Sigma^0,\Sigma^0}^{(Born)} = -C_{\eta\Lambda,\Lambda}^{(Born)} = 2D \ ,$$

$$C^{(Born)}_{\pi^+\Sigma^-,\Sigma^0} = -C^{(Born)}_{\pi^-\Sigma^+,\Sigma^0} = C^{(Born)}_{\pi^0\Sigma^+,\Sigma^+} = 2\sqrt{3}F \ ,$$

$$C^{(Born)}_{K^+\Xi^-,\Lambda} = C^{(Born)}_{K^0\Xi^0,\Lambda} = -D + 3F \ ,$$

$$\sqrt{2}C^{(Born)}_{K^+\Xi^-,\Sigma^0} = -\sqrt{2}C^{(Born)}_{K^0\Xi^0,\Sigma^0} = C^{(Born)}_{\bar{K}^0\Sigma^-,\Xi^-} = C^{(Born)}_{K^-\Sigma^+,\Xi^0} = \sqrt{6}(D+F) \ . \tag{2.13}$$

This set of Clebsch-Gordan coefficients, taken from Ref. [29], are symmetric under the combined transformation $B_1 \leftrightarrow B_2$ and $\phi \leftrightarrow \bar{\phi}$, i.e., $C_{\bar{\phi}B_1,B_2} = C_{\phi B_2,B_1}$. It should be noted that the eqs. (2.10) and (2.11) must be multiplied by a factor $[1/(2\sqrt{3}f)]$ to recover our model's notation, because it differs from that of the reference taken.

Finally, at NLO $\mathcal{O}(p^2)$, the contributions of the $\mathcal{L}^{(2)}_{\phi B}$ term to meson-baryon s-wave scattering are:

$$\begin{aligned}\mathcal{L}^{(2)}_{\phi B} =& b_D\langle\bar{B}\{\chi_+,B\}\rangle + b_F\langle\bar{B}[\chi_+,B]\rangle + b_0\{\bar{B}B\rangle\langle\chi_+\rangle + d_1\langle\bar{B}\{u_\mu,[u^\mu,B]\}\rangle \\ &+ d_2\langle\bar{B}[u_\mu,[u^\mu,B]]\rangle + d_3\langle\bar{B}u_\mu\rangle\langle u^\mu B\rangle + d_4\langle\bar{B}B\rangle\langle u^\mu u_\mu\rangle \ ,\end{aligned} \tag{2.14}$$

where the parameters preceding each term are the LECs at NLO, needed to be determined from experiment as they are not fixed by the symmetries of the underlying theory; and χ_+ is the term responsible of explicit breaking of chiral symmetry:

$$\chi_+ = -\frac{1}{4f^2}\{\phi,\{\phi,\chi\}\} \quad \text{with} \quad \chi = \begin{pmatrix} m_\pi^2 & 0 & 0 \\ 0 & m_\pi^2 & 0 \\ 0 & 0 & m_K^2 - m_\pi^2 \end{pmatrix} \ . \tag{2.15}$$

Developing each constituent of the Lagrangian:

$$\begin{aligned} b_D\langle\bar{B}\{\chi_+,B\}\rangle &= -\frac{b_D}{4f^2}\langle\bar{B}(\phi^2\chi + 2\phi\chi\phi + \chi\phi^2)B + \bar{B}B(\phi^2\chi + 2\phi\chi\phi + \chi\phi^2)\rangle \ , \\ b_F\langle\bar{B}[\chi_+,B]\rangle &= -\frac{b_F}{4f^2}\langle\bar{B}(\phi^2\chi + 2\phi\chi\phi + \chi\phi^2)B - \bar{B}B(\phi^2\chi + 2\phi\chi\phi + \chi\phi^2)\rangle \ , \\ b_0\langle\bar{B}B\rangle\langle\chi_+\rangle &= -\frac{b_0}{4f^2}\langle\bar{B}B\rangle\langle\phi^2\chi + 2\phi\chi\phi + \chi\phi^2\rangle \ , \end{aligned}$$

$$
\begin{aligned}
d_1\langle\bar{B}\{u_\mu,[u^\mu,B]\}\rangle &= \frac{2d_1}{f^2}\langle\bar{B}(\partial_\mu\phi\partial^\mu\phi B-\partial_\mu\phi B\partial^\mu\phi+\partial^\mu\phi B\partial_\mu\phi-B\partial^\mu\phi\partial_\mu\phi)\rangle \ , \\
d_2\langle\bar{B}[u_\mu,[u^\mu,B]]\rangle &= \frac{2d_2}{f^2}\langle\bar{B}(\partial_\mu\phi\partial^\mu\phi B-\partial_\mu\phi B\partial^\mu\phi-\partial^\mu\phi B\partial_\mu\phi+B\partial^\mu\phi\partial_\mu\phi)\rangle \ , \\
d_3\langle\bar{B}u_\mu\rangle\langle u^\mu B\rangle &= \frac{2d_3}{f^2}\langle\bar{B}\partial_\mu\phi\rangle\langle\partial^\mu\phi B\rangle \ , \\
d_4\langle\bar{B}B\rangle\langle u^\mu u_\mu\rangle &= \frac{2d_4}{f^2}\langle\bar{B}B\rangle\langle\partial^\mu\phi\partial_\mu\phi\rangle \ ;
\end{aligned}
\tag{2.16}
$$

the resulting expression of the potential (see (iv) in Fig. 1.1) becomes:

$$
V_{ij}^{NLO}=\frac{1}{f^2}\mathcal{N}_i\mathcal{N}_j\left[D_{ij}-2\left(w_iw_j+\frac{q_i^2q_j^2}{3(M_i+E_i)(M_j+E_j)}\right)L_{ij}\right] \ , \tag{2.17}
$$

where $w_i=\sqrt{m_i^2+q_i^2}$ is the meson energy. The D_{ij} and L_{ij} coefficients depend on the NLO parameters and have been determined using Mathematica, in the same procedure as for LO constants. They are given in Table 2.2.

All in all, adding all the equations found in this section, the total interaction kernel up to NLO can be written as:

$$
V_{ij}=V_{ij}^{WT}+V_{ij}^{DB}+V_{ij}^{CB}+V_{ij}^{NLO} \ . \tag{2.18}
$$

2.2 Bethe-Salpeter equation

As previously mentioned, a perturbative treatment of the scattering amplitude can not be employed in an energy region which contains molecular like resonances. Therefore, a non-perturbative resummation is needed. UχPT consists in solving the Bethe-Salpether (BS) equation in coupled channels for the scattering amplitudes T_{ij} using the potential derived from the chiral Lagrangian, Eq. (2.18). The BS expression, which accounts for infinite contributions of the coupled channels, corresponds to an infinite sum (see Fig. 2.1):

$$T_{ij} = V_{ij} + V_{il} G_l V_{lj} + V_{il} G_l V_{lk} G_k V_{kj} + ... = V_{ij} + V_{il} G_l T_{lj} \ , \tag{2.19}$$

where the sub-indexes $i, j, l, ...$ run over all possible channels and the loop function G_l stands for the propagator of the meson-baryon state of channel l.

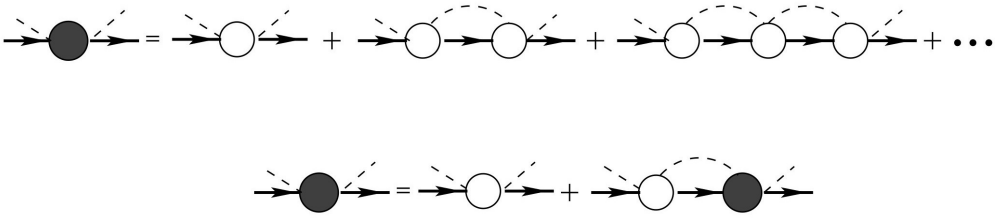

Figure 2.1: Schematic illustration of the Bethe-Salpeter equation. The scattering matrix T (interaction kernel V) is represented by the solid (empty) blobs, and the loop function G is denoted by the intermediate meson-baryon propagators.

Developing Eq. (2.19) (a more detailed discussion can be found in Ref. [26]), it can be presented in matrix form as follows:

$$T_{ij} = (1 - V_{il} G_l)^{-1} V_{lj} \ , \tag{2.20}$$

where the loop function G_l stands for a diagonal matrix with elements

$$G_l = i \int \frac{d^4 q}{(2\pi)^4} \frac{2M_l}{(P-q)^2 - M_l^2 + i\epsilon} \frac{1}{q^2 - m_l^2 + i\epsilon} \ , \tag{2.21}$$

being P the total momentum of the system. The loop function is logarithmically divergent and needs to be regularized. In this work, we will employ dimensional regularization (see Ref. [30] for details), obtaining as final expression:

$$\begin{aligned} G_l = & \frac{2M_l}{(4\pi)^2} \left[a_l(\mu) + \ln \left(\frac{M_l^2}{\mu^2} \right) + \frac{m_l^2 - M_l^2 + s}{2s} \ln \left(\frac{m_l^2}{M_l^2} \right) \right. \\ & \left. + \frac{q_l}{\sqrt{2}} \ln \left(\frac{(s + 2\sqrt{s} q_l)^2 - (M_l^2 - m_l^2)^2}{(s - 2\sqrt{s} q_l)^2 - (M_l^2 - m_l^2)^2} \right) \right] \ . \end{aligned} \tag{2.22}$$

These loop functions G_l depend on new free parameters $a_l(\mu)$, the so-called substraction constants (SCs), that replace the divergence for a given dimensional regularization scale μ which is taken to be 630 MeV, a characteristic value for this type of physics [31]. These constants are unknown, although a natural estimation can be established based on Ref. [22], and it comes out to be around -2.0. In our study, we will allow the SCs to vary between $[-3.5, -1]$. If we make a change in the regularization scale of a channel, we can reabsorb it by means of the relationship $a_l(\mu) - a_l(\mu') = 2ln(\mu'/\mu)$, which can be deduced from Eq. (2.22). In addition, isospin symmetry arguments are frequently used to reduce the number of independent SCs, which contains the states $\pi\Xi$, $\bar{K}\Lambda$, $\bar{K}\Sigma$ and $\eta\Xi$ for $I = 1/2$ and the states $\pi\Xi$ and $\bar{K}\Sigma$ for $I = 3/2$. For the particular $I = 1/2$ case needed in the present study, we have four different SCs, namely $a_{\pi\Xi}$, $a_{\bar{K}\Lambda}$, $a_{\bar{K}\Sigma}$ and $a_{\eta\Xi}$.

With the T-matrix obtained, one can look for resonances. These appear as matrix-singularities, and according to Eq. (2.20), they correspond to the zeros in the complex plane of $(1 - V_{il}G_l)^{-1}$. We search for poles ($z_p = M_R - i\Gamma_R/2$) of the scattering amplitude in the second Riemann sheet (RS) of the complex energy plane, whose real and imaginary parts correspond to its mass (M_R) and half width ($\Gamma_R/2$). To determine the RS of the amplitude, since the loop function is expressed in terms of the relative momentum of the two-body system (Eq. 2.22), a reflection on momentum ($q_l \to -q_l$) must be taken into account. Thus, the rotation to the second RS of the loop function for a general complex value of $\sqrt{s}$ is as follows:

$$G_l^{II}(\sqrt{s}) = G_l(\sqrt{s}) + i2M_l\frac{q_l}{4\pi\sqrt{s}} \ , \tag{2.23}$$

which will be carried out as long as the real part of the complex energy is greater than the threshold of the corresponding channel.

Once the z_p pole is located, the scattering amplitude in the proximity of this pole on the real axis behaves as:

$$T_{ij}(\sqrt{s}) \sim \frac{g_i g_j}{\sqrt{s} - z_p} \ , \tag{2.24}$$

where the complex coupling strengths (g_i, g_j) of the resonance to the corresponding meson-baryon channels can be extracted from the residue of the pole.

2.3 Analysis of resonances

Applying the formalism explained, in Ref. [21] we were able to dynamically generate the $\Xi(1620)$ and $\Xi(1690)$ poles exhibiting a high degree of agreement with the resonance positions and widths, and being able to naturally explain the puzzle with the decay branching ratios of the $\Xi(1690)$. The 10 parameters of the model $(f, D, F, b_D, b_F, b_0, d_1, d_2, d_3, d_4)$ were fixed to the ones obtained in the neutral $S = -1$ sector from the BCN model (see Table II in Ref. [25]), since there was little experimental data available in $S = -2$ to fit them correctly. This highlights the power of UχPT where it is possible to extend the same Lagrangian as the one used in such reference due to the $SU(3)$ symmetry.

Thus, the strategy followed was to vary the SCs within a reasonable natural size range, from -3.5 to -1, to describe the masses of the $\Xi(1620)$ and $\Xi(1690)$ states in the best possible way. This procedure was called Model I in that work. Using the corresponding parametrization from Table 2.3, the results set out in Table 2.4 showed an energy location of both poles within the experimental error band (Eq. (1.1), (1.2)). Moreover, the value of the theoretical width of $\Xi(1690)$ lied within the error band. This was in contrast to the theoretical width of $\Xi(1620)$ which was about a factor of 2.5 larger than the nominal value.

As a next step, we decided to modify the global scale factor f, yet within the corresponding error bars of the BCN model, this being Model II. This constant takes into account the role of the $\bar{K}$'s and η's in the system, and since in the $S = -2$ sector each pseudoscalar meson has a higher relevance over π's than in the $S = -1$ sector, it was reasonable to expect a slightly larger value for f. On the other hand, the corresponding SCs barely differed from those of Model I. These combined modifications provided however a notable improvement of the pole locations, as shown in Table 2.4. The theoretical masses reached values closer to the nominal ones, the same could be said for the theoretical $\Xi(1690)$ width. Regarding the $\Xi(1620)$ width for Model II, the

new value exceeded by 10 MeV that of Model I.

As a last study, we addressed the issue of the $\Xi(1690)$ decay branching ratios. For a general two-body decay, the partial width of an s-wave resonance with mass M_R in the ith-channel is proportional to $\Gamma_R^i \sim q_i |g_{R,i}|^2 M_i / M_R$, where q_i is the momentum of the outgoing particle in the rest frame of the parent particle, and $g_{R,i}$ represents the coupling of the resonance to the corresponding channel [2]. Then, using the corresponding coupling from Table 2.4, we computed the $\Xi(1690)$ branching ratios for Model II [21]:

$$B_1 = \frac{\Gamma^{\pi\Xi}_{\Xi(1690)}}{\Gamma^{\bar{K}\Sigma}_{\Xi(1690)}} = \frac{\Gamma^{\pi^+\Xi^-}_{\Xi(1690)} + \Gamma^{\pi^0\Xi^0}_{\Xi(1690)}}{\Gamma^{\bar{K}^-\Sigma^+}_{\Xi(1690)} + \Gamma^{\bar{K}^0\Sigma^0}_{\Xi(1690)}} = 0.25 \ , \tag{2.25}$$

$$B_2 = \frac{\Gamma^{\bar{K}\Sigma}_{\Xi(1690)}}{\Gamma^{\bar{K}^0\Lambda}_{\Xi(1690)}} = \frac{\Gamma^{K^-\Sigma^+}_{\Xi(1690)} + \Gamma^{\bar{K}^0\Sigma^0}_{\Xi(1690)}}{\Gamma^{\bar{K}^0\Lambda}_{\Xi(1690)}} = 1.6 \ . \tag{2.26}$$

As it can be seen, the values are not only of the same order of magnitude as the experimental data [3], but also, in the case of B_2, the branching ratio is within the nominal range.

Thus, having demonstrated in Ref. [21] the importance of considering Born and NLO contributions for precise resonance calculations, our current focus will be on exploring whether our model can effectively explain the final state interaction in the nonleptonic $\Xi_c^+ \to \pi^+\pi^+\Xi^-$ weak process. The formalism describing this decay will be presented in the following section.

[2] When a threshold position is close to a resonance, as in the case of the $\bar{K}\Sigma$ thresholds for the $\Xi(1690)$ resonance, the effect of the finite width of the resonance on the partial decay width needs to be taken into account by convoluting the spectral function of the resonance (as described in Eq. 17 in Ref. [32]).

D_{ij}	$\pi^+\Xi^-$	$\pi^0\Xi^0$	$\bar{K}^0\Lambda$	$K^-\Sigma^+$	$\bar{K}^0\Sigma^0$	$\eta\Xi^0$
$\pi^+\Xi^-$	$2(2b_0+b_D-b_F)m_\pi^2$	0	$-(b_D-3b_F)\mu_1^2/\sqrt{6}$	0	$(b_D+b_F)\mu_1^2/\sqrt{2}$	$2\sqrt{2}(b_D-b_F)m_\pi^2/\sqrt{3}$
$\pi^0\Xi^0$		$4(b_0+b_D-b_F)m_\pi^2$	$(b_D-3b_F)\mu_1^2/2\sqrt{3}$	$(b_D+b_F)\mu_1^2/\sqrt{2}$	$(b_D+b_F)\mu_1^2/2$	$-2(b_D-b_F)m_\pi^2/\sqrt{3}$
$\bar{K}^0\Lambda$			$2(6b_0+5b_D)m_K^2/3$	$2\sqrt{2}b_Dm_K^2/\sqrt{3}$	$-2b_Dm_K^2/\sqrt{3}$	$(b_D-3b_F)\mu_2^2/6$
$K^-\Sigma^+$				$2(2b_0+b_D+b_F)m_K^2$	$-2\sqrt{2}b_Fm_K^2$	$-(b_D+b_F)\mu_2^2/\sqrt{6}$
$\bar{K}^0\Sigma^0$					$2(2b_0+b_D)m_K^2$	$(b_D+b_F)\mu_2^2/2\sqrt{3}$
$\eta\Xi^0$						$2(2b_0\mu_3^2+b_D\mu_4^2+b_F\mu_5^2)/3$

L_{ij}	$\pi^+\Xi^-$	$\pi^0\Xi^0$	$\bar{K}^0\Lambda$	$K^-\Sigma^+$	$\bar{K}^0\Sigma^0$	$\eta\Xi^0$
$\pi^+\Xi^-$	$-d_1+d_2+2d_4$	0	$\sqrt{3}(d_1-d_2)/\sqrt{2}$	$-2d_2+d_3$	$(d_1+3d_2)/\sqrt{2}$	$-\sqrt{2}(d_1-3d_2)/\sqrt{3}$
$\pi^0\Xi^0$		$-d_1+d_2+2d_4$	$-(d_1-3d_2)/2\sqrt{3}$	$(d_1+d_2)/\sqrt{2}$	$-(d_1+d_2)/2$	0
$\bar{K}^0\Lambda$			$(d_1+3d_2+2d_4)/2$	$\sqrt{6}d_2$	$-\sqrt{3}d_2$	0
$K^-\Sigma^+$				0	$-\sqrt{2}d_1$	$-(d_1+3d_2)/\sqrt{6}$
$\bar{K}^0\Sigma^0$					d_2+2d_4	$(d_1+3d_2)/2\sqrt{3}$
$\eta\Xi^0$						$d_1+3d_2+2d_4$

Table 2.2: D_{ij} and L_{ij} coefficients in the NLO potential of the pseudoescalar meson and the fundamental baryon octet with strangeness $S=-2$ and charge $Q=0$. The coefficients are symmetric, $D_{ji}=D_{ij}$ and $L_{ji}=L_{ij}$. With the definitions: $\mu_1^2=m_K^2+m_\pi^2$, $\mu_2^2=5m_K^2-3m_\pi^2$, $\mu_3^2=4m_K^2-m_\pi^2$, $\mu_4^2=8m_K^2-3m_\pi^2$, $\mu_5^2=8m_K^2-5m_\pi^2$.

	Model I	Model II
$a_{\pi\Xi}$	-2.7981	-2.7228
$a_{\bar{K}\Lambda}$	-1.0071	-1.0000
$a_{\bar{K}\Sigma}$	-3.0938	-2.9381
$a_{\eta\Xi}$	-3.2665	-3.3984
f/f_π	1.196 (fixed [25])	1.204

Table 2.3: Values of the parameters for the different models described in Ref. [21]. The value of the pion decay constant is $f_\pi = 93$ MeV and the subtraction constants are taken at a regularization scale $\mu = 630$ MeV.

	Model I				Model II			
	$\Xi(1620)$		$\Xi(1690)$		$\Xi(1620)$		$\Xi(1690)$	
M [MeV]	1599.95		1683.04		1608.51		1686.17	
Γ [MeV]	158.88		11.51		170.00		29.72	
	g_i	$\lvert g_i\rvert$	g_i	$\lvert g_i\rvert$	g_i	$\lvert g_i\rvert$	g_i	$\lvert g_i\rvert$
$\pi^+\Xi^-$	$1.70 + i0.78$	1.87	$0.44 + i0.07$	0.45	$1.73 + i0.85$	1.93	$0.51 + i0.25$	0.57
$\pi^0\Xi^0$	$-1.22 - i0.62$	1.37	$0.08 - i0.10$	0.13	$-1.24 - i0.67$	1.41	$0.09 - i0.06$	0.11
$\bar{K}^0\Lambda$	$-2.11 - i0.08$	2.11	$0.50 - i0.06$	0.51	$-2.12 - i0.09$	2.12	$0.81 - i0.02$	0.81
$K^-\Sigma^+$	$0.81 - i0.22$	0.84	$1.0 - i0.16$	1.01	$0.8 - i0.25$	0.84	$1.36 + i0.10$	1.36
$\bar{K}^0\Sigma^0$	$-0.41 + i0.28$	0.50	$-1.34 + i0.26$	1.37	$-0.36 + i0.31$	0.48	$-1.99 + i0.08$	1.99
$\eta\Xi^0$	$-0.23 + i0.13$	0.26	$-0.74 + i0.13$	0.76	$-0.20 + i0.12$	0.24	$-1.04 + i0.06$	1.04

Table 2.4: Comparison of the pole positions between Model I and Model II, conducted in Ref. [21], with their couplings g_i and the corresponding modulus found in $J^P = \frac{1}{2}^-$, $(I, S) = (\frac{1}{2}, -2)$.

Chapter 3

The $\Xi_c^+ \to \pi^+\pi^+\Xi^-$ decay model

The analysis of the Ξ_c^+ decay into $\pi^+\pi^+\Xi^-$ is a particularly suitable reaction for studying strange Ξ baryons. The process involves the $c \to s$ weak transition and the production of a high-momentum π^+, followed by an hadronization process where intermediate meson-baryon pairs are formed with certain weights. These new states then re-scatter through strong interactions, taking into account the coupled-channel chiral unitary scheme discussed in the previous section, resulting in the final meson-baryon state of interest.

3.1 Weak process

At the quark level, the $q \to q'$ weak transition at the Wqq' vertices is determined by the strength of the different Cabibbo-Kobayashi-Maskawa (CKM) matrix elements [33]. The dominant CKM diagram for the Ξ_c^+ decay, when a high-momentum π^+ emission is required, is depicted in Fig. 3.1. We can see the W-exchange weak process transforming the c quark into $su\bar{d}$, where a π^+ particle and a sus quark state are formed. This mechanism is preferred due to its favourable colour recombination factor for the outgoing quarks in the W boson, in which all the colours are allowed. On the other hand, the u and s quarks in the Ξ_c^+ form a strongly correlated antisymmetric diquark configuration which is difficult to separate. Moreover, the kinematics also favour this unique quark-line diagram since we are interested in situations where the outgoing meson-baryon pair occurs at low invariant masses, which requires the emission of a high momentum π^+ (more comprehensive explanations are refered in [34]).

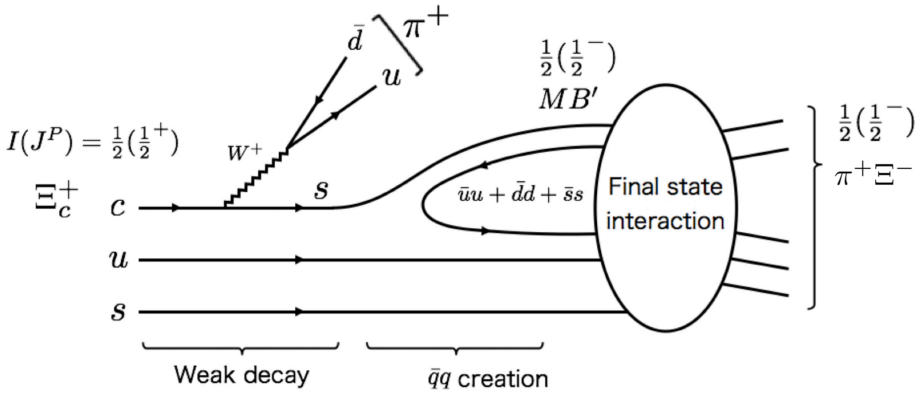

Figure 3.1: Dominant quark-line diagram for the $\Xi_c^+ \to \pi^+\pi^+\Xi^-$ decay. The full (serrated) lines correspond to quarks (the W boson).

3.2 Hadronization

The next step is the hadronization of the *sus* cluster formed after the charm quark decay by introducing a vacuum-quantum-numbers $\bar{q}q$ pair from the Fermi sea, $\bar{u}u + \bar{d}d + \bar{s}s$, to construct the intermediate meson-baryon state MB'.

Although weak interaction allows for isospin violation, this is a process in which the virtual three-quark state (*sus*) conserves its isospin. Since the original $\Xi_c^+(cus)$ has $I = 1/2$ and knowing that $I(u) = 1/2$ and $I(c) = I(s) = 0$, from the quark model we can see that the *us* diquark keeps the $I = 1/2$ configuration. Consequently, the cluster is filtered with an isospin of $1/2$. Furthermore, since hadronization is considered a strong interaction process, the MB' also appears with $I = 1/2$. Additionally, assuming ground states and a relative s-wave ($L = 0$) for the final $\pi^+\Xi^-$ pair, with quantum numbers $\pi^+(0^-)$ and $\Xi^-(1/2^+)$, the original *sus* quark state must have $J^P = 1/2^-$. Coupled with the fact that the *us* quarks has the same quantum numbers as the Ξ_c^+ state ($J^P = 1/2^+$ each), the s quark originated in the weak decay must carry the negative parity, being an excited state which would correspond to an $L = 1$ orbit of a potential well. All these considerations lead us to conclude that the s quark must actively participate in the hadronization process to reach the ground state of the final system ($L = 0$).

On the other hand, due to the strong correlation of the u and s quarks in the Ξ_c^+, they will act as spectators in Fig. 3.1. They will be at rest in the Ξ_c^+ center-of-mass frame and, therefore, after hadronization they will form the intermediate baryon, while the s quark originated in the weak interaction will be part of the meson.

The process is going to be studied by using flavour descomposition of states. We start with the initial Ξ_c^+ baryon state [35]:

$$|\Xi_c^+\rangle = \frac{1}{\sqrt{2}}\,|c(su-us)\rangle \quad , \tag{3.1}$$

which turns after the weak process into

$$\frac{1}{\sqrt{2}}\,|s(su-us)\rangle \quad . \tag{3.2}$$

Thus, we introduce the Fermi sea of quarks to carry out hadronization,

$$|H\rangle = \frac{1}{\sqrt{2}}\,|s(\bar{u}u+\bar{d}d+\bar{s}s)(su-us)\rangle = \frac{1}{\sqrt{2}}\sum_{i=1}^{3}|P_{3i}q_i(su-us)\rangle \quad , \tag{3.3}$$

where we have defined

$$P = \begin{pmatrix} u\bar{u} & u\bar{d} & u\bar{s} \\ d\bar{u} & d\bar{d} & d\bar{s} \\ s\bar{u} & s\bar{d} & s\bar{s} \end{pmatrix} \quad \text{and} \quad q = \begin{pmatrix} u \\ d \\ s \end{pmatrix} \quad . \tag{3.4}$$

The P matrix can be understood as the quark-antiquark representation of the $SU(3)$ pseudoscalar meson matrix

$$P = \begin{pmatrix} \frac{\pi^0}{\sqrt{2}} + \frac{\eta}{\sqrt{3}} + \frac{\eta'}{\sqrt{6}} & \pi^+ & K^+ \\ \pi^- & -\frac{\pi^0}{\sqrt{2}} + \frac{\eta}{\sqrt{3}} + \frac{\eta'}{\sqrt{6}} & K^0 \\ K^- & \bar{K}^0 & -\frac{\eta}{\sqrt{3}} + \frac{2\eta'}{\sqrt{6}} \end{pmatrix} \quad , \tag{3.5}$$

where the mixing of the singlet and octet $SU(3)$ states for the η, η' has been assumed [36]:

$$\eta = \frac{1}{3}\eta_1 + \frac{2\sqrt{2}}{3}\eta_8 \quad , \qquad \eta' = \frac{2\sqrt{2}}{3}\eta_1 - \frac{1}{3}\eta_8 \quad . \tag{3.6}$$

Hence, the hadronized state becomes:

$$|H\rangle = \frac{1}{\sqrt{2}}\left(K^- u(su-us) + \bar{K}^0 d(su-us) + \left(-\frac{\eta}{\sqrt{3}} + \frac{2\eta'}{\sqrt{6}}\right) s(su-us)\right) \quad . \tag{3.7}$$

Now, we proceed in a similar way to introduce the baryons, where we use the following relation extracted from Ref. [34]:

$$\begin{aligned} B =& \frac{1}{\sqrt{2}} \begin{pmatrix} u(ds-sd) & u(su-us) & u(ud-du) \\ d(ds-sd) & d(su-us) & d(ud-du) \\ s(ds-sd) & s(su-us) & s(ud-du) \end{pmatrix} \\ =& \begin{pmatrix} \frac{\Sigma^0}{\sqrt{2}} + \frac{\Lambda}{\sqrt{6}} + \frac{\Lambda_1}{\sqrt{3}} & \Sigma^+ & p \\ \Sigma^- & -\frac{\Sigma^0}{\sqrt{2}} + \frac{\Lambda}{\sqrt{6}} + \frac{\Lambda_1}{\sqrt{3}} & n \\ \Xi^- & \Xi^0 & -\frac{2\Lambda}{\sqrt{6}} + \frac{\Lambda_1}{\sqrt{3}} \end{pmatrix} \quad . \end{aligned} \tag{3.8}$$

Consequently,

$$|H\rangle = |K^-\Sigma^+\rangle + |\bar{K}^0\left(-\frac{\Sigma^0}{\sqrt{2}} + \frac{\Lambda}{\sqrt{6}} + \frac{\Lambda_1}{\sqrt{3}}\right)\rangle + |\left(-\frac{\eta}{\sqrt{3}} + \frac{2\eta'}{\sqrt{6}}\right)\Xi^0\rangle \quad ; \tag{3.9}$$

and, neglecting the η' and Λ_1 hadrons because of their large masses which would lead to a small contribution, we obtain the intermediate state as

$$|MB'\rangle = |K^-\Sigma^+\rangle - \frac{1}{\sqrt{2}}|\bar{K}^0\Sigma^0\rangle + \frac{1}{\sqrt{6}}|\bar{K}^0\Lambda\rangle - \frac{1}{\sqrt{3}}|\eta\Xi^0\rangle \quad , \tag{3.10}$$

where the coefficients preceding each possible state are their corresponding weights, h_i. Particularly,

$$\begin{aligned} h_{\pi^0\Xi^0} = h_{\pi^+\Xi^-} = 0\,, \quad h_{\bar{K}^0\Lambda} = \frac{1}{\sqrt{6}}\,, \\ h_{K^-\Sigma^+} = 1\,, \quad h_{\bar{K}^0\Sigma^0} = -\frac{1}{\sqrt{2}}\,, \quad h_{\eta\Xi^0} = -\frac{1}{\sqrt{3}}\ . \end{aligned} \tag{3.11}$$

As mentioned before, the s quark originated after the weak decay becomes part of the intermediate meson. This is why, as we can see, direct production of the $\pi\Xi$ pairs is not possible since the π particle does not contain that quark. However, this channel will be present in the final interaction through intermediate loops, as will be explained below.

3.3 Final-state interaction

After the production of the intermediate mesons and baryons, they re-scatter into the final $\pi^+\Xi^-$ state, which is parametrized by the decay amplitude $\mathcal{M}_{\pi^+\Xi^-}$. The diagrammatic representation is depicted in Fig. 3.2, where the total contribution is the sum of the direct tree-level process (i.e., the final state is directly produced from the $q\bar{q}$ creation) and the final-state interaction contribution of the intermediate meson-baryon pairs.

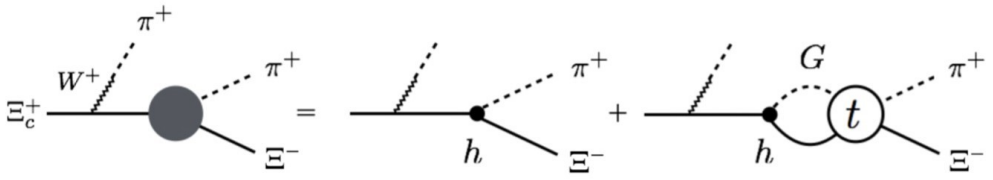

Figure 3.2: Schematic diagram of the decay amplitude for $\Xi_c^+ \to \pi^+\pi^+\Xi^-$. The first term in the right-hand side stands for the tree-level contributions, whereas the second one contains the meson-baryon loop function G involving the intermediate meson-baryon states along with their associated weights h, and the scattering amplitude t.

Mathematically,

$$\mathcal{M}_{\pi^+\Xi^-}(M_{\text{inv}}) = V_P \left(h_{\pi^+\Xi^-} + \sum_i h_i G_i(M_{\text{inv}}) t_{i,\pi^+\Xi^-}(M_{\text{inv}}) \right) \quad , \tag{3.12}$$

where the loop function G_i contemplates any of the possible intermediate states (see Eq. 3.10), with its corresponding weight h_i (Eq. 3.11), whose interaction will produce the final $\pi^+\Xi^-$ pair described through the scattering amplitude $t_{i,\pi^+\Xi^-}$. M_{inv} is the invariant mass of the meson–baryon system in the final state and V_P is a factor that

incorporates the probability of the initial weak decay process as well the hadronization process. However, as knowing the precise value of V_p is a complex task, in the present study it will be taken as a constant, following Ref. [25, 34], neglecting its M_{inv} dependence. It should be noted that in the energy range of interest, the factors required to describe the interaction exhibit smooth behavior compared to the changes induced by these interactions, validating the assumption made (this conduct is shown in Fig. 3 of Ref. [37]).

At this point, it is relevant to mention that the chiral model presented in Chapter 2 dynamically describes the $\Xi(1620)$ and $\Xi(1690)$ resonances for the final state interaction in the $\pi^+\Xi^-$ channel, which are located in the region of invariant masses M_{inv} accessible through the decay of the Ξ_c^+ fixed by kinematics relations:

$$M_{\text{inv}}^{\text{min}} = m_{\pi^+} + M_{\Xi^-} = 1460.89 \text{ MeV} \tag{3.13}$$

$$M_{\text{inv}}^{\text{max}} = M_{\Xi_c^+} - m_{\pi_{\text{ext}}^+} = 2328.14 \text{ MeV} \tag{3.14}$$

Consequently, upon examining this ranging of M_{inv}, we also find the $\Xi(1530)$ state that could be significantly coupled to $\pi\Xi$ pairs (see Fig. 3.3).

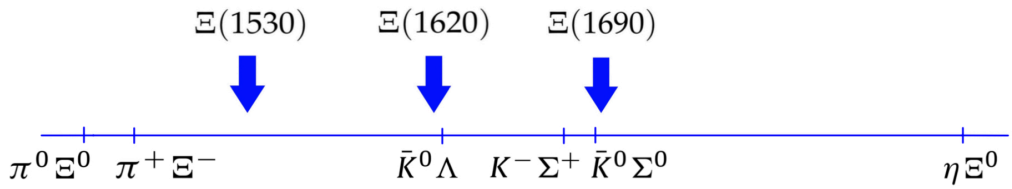

Figure 3.3: Schematic representation of the channel thresholds with strangeness $S = -2$ and charge $Q = 0$, indicating the energy positions of the possible Ξ^* states that can be observed within this range: the $\Xi(1530)$, $\Xi(1620)$ and $\Xi(1690)$ resonances.

This particular resonance is widely known in the PDG compilation [3] with a four-star rating and an average width of $\Gamma = 9.1 \pm 0.5$ MeV. It has been observed in the $\Lambda^+ \to K^+\pi^+\Xi^-$ decay, allowing us to conclusively assign a value of $I(J^P) = 1/2(3/2^+)$ to this excited state. Furthermore, the experimental data from

Belle Collaboration [7] confirms the prominent signal of this resonance in our decay process of interest, $\Xi_c^+ \to \pi^+\pi^+\Xi^-$, as illustrated in Fig. 3.4.

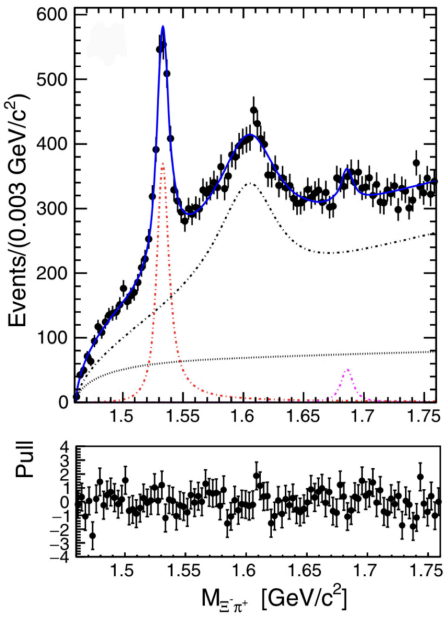

Figure 3.4: The $M_{\pi\Xi^-}$ spectrum in the Ξ_c^+ signal region (points with errorbars), from [7]. The fit results (solid blue line) are also shown, taking into account the resonances associated with $\Xi(1530)$ (dashed red line), $\Xi(1620)$ (dot-dashed black line) including a nonresonant contribution, and $\Xi(1690)$ (dot-dashed pink line), and the combinatorial background (dotted black line). To provide a measure of the discrepancy between the fitted values and the observed data points, the bottom plot displays the normalized residuals of the fit; indicating a good consistency as they are distributed close to zero.

Hence, since our model cannot account for resonances with quantum numbers $J^P = 3/2^+$, we will explore the possibility of explicitly including the contribution of the $\Xi(1530)$ state in the final amplitude using a Breit-Wigner form:

$$\begin{aligned}\mathcal{M}_{\pi^+\Xi^-}(M_{\text{inv}}) = V_P \Bigg(& h_{\pi^+\Xi^-} + \sum_i h_i G_i(M_{\text{inv}}) t_{i,\pi^+\Xi^-}(M_{\text{inv}}) \\ & + \alpha \frac{M_{\Xi^*(1530)}}{M_{\text{inv}} - M_{\Xi^*(1530)} + i\frac{\Gamma_{\Xi^*(1530)}}{2}} \Bigg) \ ,\end{aligned} \tag{3.15}$$

where α is a dimensionless complex parameter that determines the weight of the

$\Xi(1530)$ contribution.

With the above decay amplitude, we can calculate the partial decay width:

$$\Gamma_{\pi^+\Xi^-} = \int_{M_{\rm inv}^{\rm min}}^{M_{\rm inv}^{\rm max}} d\Pi_3 |\mathcal{M}_{\pi^+\Xi^-}|^2 \ , \tag{3.16}$$

where $d\Pi_3$ represents the three-body phase space.

The invariant mass distribution is obtained by differentiating the width by $M_{\rm inv}$:

$$\frac{d\Gamma_{\pi^+\Xi^-}}{dM_{\rm inv}} = \frac{1}{(2\pi)^3} \frac{q_{\pi_H^+} q_{\pi_L^+} M_{\Xi^-}}{M_{\Xi_c^+}} |\mathcal{M}_{\pi^+\Xi^-}|^2 \tag{3.17}$$

with

$$q_{\pi_H^+} = \frac{\sqrt{(M_{\Xi_c^+}^2 - (m_{\pi^+} + M_{\rm inv})^2)(M_{\Xi_c^+}^2 - (m_{\pi^+} - M_{\rm inv})^2)}}{2M_{\Xi_c^+}} \ , \tag{3.18}$$

$$q_{\pi_L^+} = \frac{\sqrt{(M_{\rm inv}^2 - (m_{\pi^+} + M_{\rm inv})^2)(M_{\Xi_c^+}^2 - (m_{\pi^+} - M_{\rm inv})^2)}}{2M_{\rm inv}} \tag{3.19}$$

being, respectively, the three-momentum of the π^+ emitted in the weak decay part in the Ξ_c^+ rest frame and the three-momentum of the meson in the final $\pi^+\Xi^-$ state in the $\pi^+\Xi^-$ rest frame [1].

It is important to mention that the final $M_{\rm inv}$ distribution corresponds to the π^+ with the lower momentum, π_L^+. When combining the Ξ^- with the two π^+ candidates, the resonances can only appear in the $M_{\pi_L^+\Xi^-}$ spectrum, as illustrated in the Dalitz plot (Fig. 3.5). This observation is further supported by the findings presented in Fig. 3.6, which showcases the experimental study conducted by the Belle Collaboration [7]. Both distributions exhibit minimal overlap, with the peaks of the $\Xi(1530)$, $\Xi(1620)$ and $\Xi(1690)$ resonances clearly evident in the $M_{\pi_L^+\Xi^-}$ distribution. Conversely, only a reflection of $\Xi(1530)$ decays is observed around 2.2 GeV/c^2 in the $M_{\pi_H^+\Xi^-}$ one.

[1] Detailed formalism regarding kinematics of three-body decays are worked out in pp. 260-261 of Ref. [28].

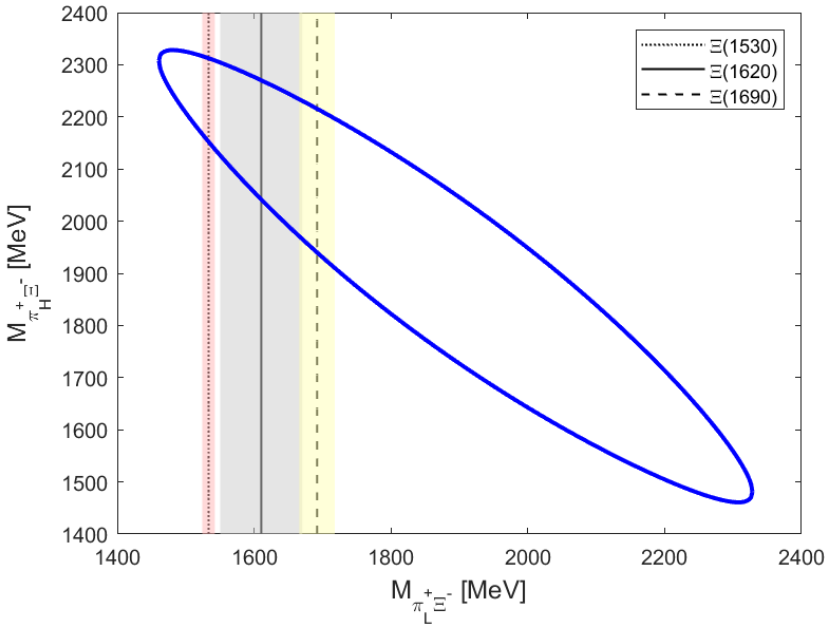

Figure 3.5: Dalitz plot for $M_{\pi_L^+\Xi^-}$ as a function of $M_{\pi_H^+\Xi^-}$ representing the available phase space of the $\Xi_c^+ \to \pi^+\pi^+\Xi^-$ decay. The known resonances (discontinuous lines) that appear in the final $\pi^+\Xi^-$ state are shown, with the shaded areas indicating their corresponding widths.

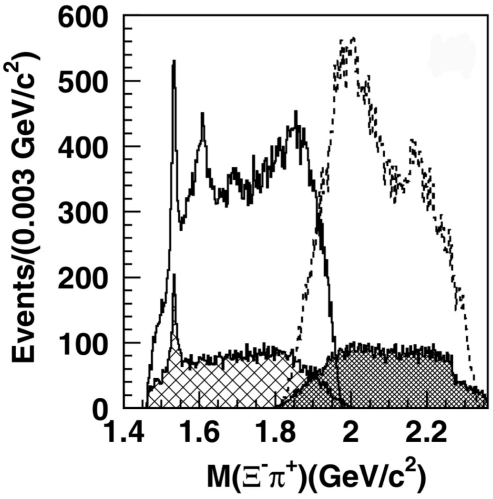

Figure 3.6: The $M_{\pi_L^+\Xi^-}$ (solid) and $M_{\pi_H^+\Xi^-}$ (dashed) distributions in the Ξ_c^+ signal region, as well as the corresponding distributions (hatched) in the Ξ_c^+ sideband region. The figure is extracted from [7].

Chapter 4

Results

This work can be seen as an attempt to improve our model used in Ref. [21]. The latest availability of experimental data at $S = -2$, provided by the Belle collaboration, has allowed the observation of signals from the $\Xi(1620)$ and $\Xi(1690)$ resonances in the final $\pi^+\Xi^-$ state via our decay of interest, with statistical significances of 25σ and 4.0σ, respectively [7].

In Chapter 3, we have shown how we can calculate the invariant mass distributions of the $\pi^+\Xi^-$ system. Consequently, with this theoretical model, we can now more precisely refit all the parameters of the Lagrangian, some of which were fixed based on the results obtained in the BCN model fixed at $S = -1$ [25], taking advantage of $SU(3)$ symmetry.

We would like to express our gratitude to Prof. M. Sumihama for granting us access to the Belle data, particularly the invariant mass spectrum. The experimental researchers made great efforts in removing the background, by subtracting data from the Ξ_c^+ sideband region (Fig. 2b in Ref. [7]) from those obtained in the signal region (Fig. 2a in Ref. [7]). This allows us to avoid including any additional background contributions (dotted black line in Fig. 3.4) in our theoretical model. Hence, this spectrum (shown in Fig. 4.1) ideally should be fully explained by our invariant amplitude (Eq. 3.17).

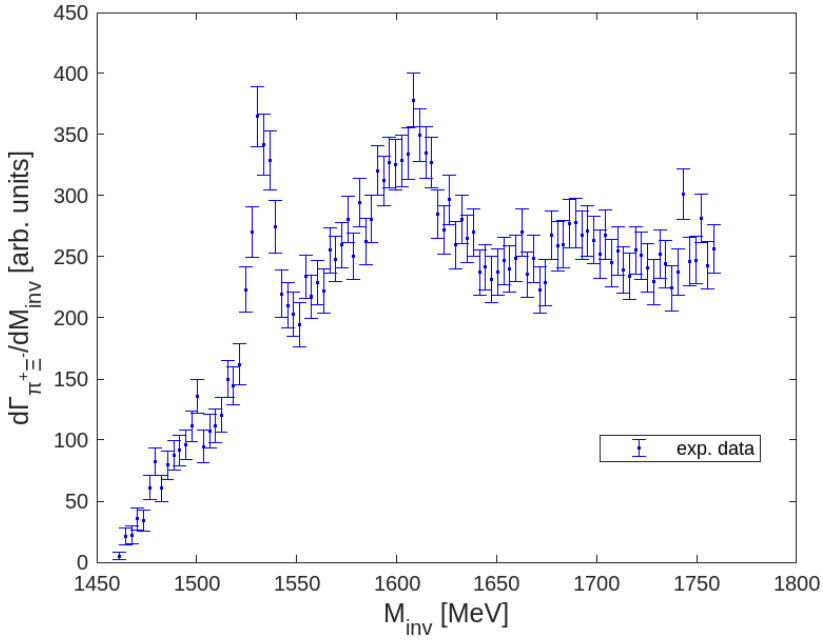

Figure 4.1: Data sample from the Belle Collaboration [7] showing the $\pi^+\Xi^-$ invariant mass distribution "without background" in the Ξ_c^+ signal region.

4.1 Fitting procedure and data treatment

In the context of $U\chi PT$, the $S = -2$ sector offers us a new good opportunity to extract information on the parameters that are present in the model: the meson decay constant f, the axial vector couplings D and F, the NLO coefficients $b_0, b_D, b_F, d_1, d_2, d_3, d_4$; the subtraction constants $a_{\pi\Xi}, a_{\bar{K}\Lambda}, a_{\bar{K}\Sigma}, a_{\eta\Xi}$; the factor V_p of the final-state interaction and the α parameter of the $\Xi(1530)$ resonant mechanism.

From the data sample comprising 980 f^{-1} of e^+e^- collisions at the KEKB asymmetric (3.5 on 8 GeV) accelerator, collected by the Belle detector [38], we performed parameter fitting employing the sophisticated tool known as MINUIT. Developed by CERN, MINUIT enables the determination of optimal parameter values for a theoretical model by fitting them to experimental data. In our specific case, this involves numerically minimizing an objective function that quantifies the discrepancy between theoretical predictions of the invariant mass distribution and experimental observations, using the method of least squares. The standard fitting procedure consists of finding the values of the 17 parameters of our chiral model that give the lowest value

of chisquare, χ^2, per degree of freedom ($\chi^2_{\text{d.o.f}}$):

$$\chi^2_{\text{d.o.f}} = \frac{1}{\text{d.o.f.}} \sum_{i=1}^{n} \frac{(y_i^{th} - y_i^{\text{exp}})^2}{\sigma_i^2} \tag{4.1}$$

where y_i^{th}, y_i^{exp} and σ_i^2 represent, respectively, the experimental value, theoretical prediction and error of the i^{th} point out of 100. The degrees of freedom (d.o.f.) are the total experimental points minus the free parameters to adjust.

For the initialization of MINUIT, it is required to set input values for the parameters, as well as limits to prevent them from taking unphysical values. As a starting point, we will use the values established in Model 2 of our previous work [21], taking their respective associated error bars (see the first column of Table 4.1). Once the fitting process is carried out, we generate variations around the central values of the existing parameters, using the previously obtained parametrization. This involves exploring different combinations of parameter values to find the global minimum of the $\chi^2_{\text{d.o.f}}$ function and, thus, obtain the best possible fit to the experimental data [1]. The obtained results are displayed in the second column of Table 4.1, referred to as Model A.

This new parametrization significantly improves the fitting of the SCs towards their natural size. Interestingly, the remaining parameters approach their respective limit values. The decay constant f tends towards its upper maximum, while the axial vector couplings move towards their lowest error bars, resulting in a significant discrepancy in their sum compared to the reference value of $g_A = D + F = 1.26 \pm 0.05$. Nevertheless, the final $\chi^2_{\text{d.o.f}}$ is not far from unity, indicating a high level of overall agreement with the experimental data as shown in Appendix I, Fig. I. One can clearly see the two peaks corresponding to the $\Xi(1620)$ and $\Xi(1690)$ resonances, as well as the explicit inclusion of the $\Xi(1530)$ resonant term with $J^P = 3/2^+$.

[1] It is important to note that the optimal value may not be unique, especially in complicated problems with multiple local minima in the objective function. In such cases, the minimization may converge to a local minimum instead of the global minimum. Therefore, it is essential to perform a careful exploration of the parameter space and assess the stability of the obtained results.

	Model 2 (from [21])	Model A (1σ)	Model B (2σ)	Model C (no limits)
$a_{\pi\Xi}$	-2.7228	$-2.6703 \pm 6 \cdot 10^{-6}$	-2.6887 ± 0.0713	$-1.2302 \pm 8 \cdot 10^{-6}$
$a_{\bar{K}\Lambda}$	-1.0000	$-1.8658 \pm 3 \cdot 10^{-6}$	-2.0873 ± 0.1212	$-1.4011 \pm 3 \cdot 10^{-6}$
$a_{\bar{K}\Sigma}$	-2.9381	$-1.3112 \pm 3 \cdot 10^{-6}$	-1.4821 ± 0.0252	$-2.9452 \pm 5 \cdot 10^{-6}$
$a_{\eta\Xi}$	-3.3984	$-2.2348 \pm 7 \cdot 10^{-6}$	-2.2220 ± 0.1054	$-2.1954 \pm 4 \cdot 10^{-6}$
f/f_π	$1.204^{+0.005}_{-0.015}$	$1.209 \pm 4 \cdot 10^{-10}$	1.222 ± 0.005	$1.2297 \pm 2 \cdot 10^{-6}$
b_0 [GeV^{-1}]	$0.129^{+0.032}_{-0.032}$	$0.161 \pm 4 \cdot 10^{-9}$	0.193 ± 0.012	$0.410 \pm 3 \cdot 10^{-6}$
b_D [GeV^{-1}]	$0.120^{+0.010}_{-0.09}$	$0.130 \pm 10 \cdot 10^{-10}$	0.140 ± 0.004	$-0.059 \pm 6 \cdot 10^{-6}$
b_F [GeV^{-1}]	$0.209^{+0.022}_{-0.026}$	$0.231 \pm 7 \cdot 10^{-8}$	0.253 ± 0.013	$1.061 \pm 6 \cdot 10^{-6}$
d_1 [GeV^{-1}]	$0.151^{+0.021}_{-0.027}$	$0.124 \pm 7 \cdot 10^{-10}$	0.097 ± 0.005	$-1.903 \pm 6 \cdot 10^{-6}$
d_2 [GeV^{-1}]	$0.126^{+0.012}_{-0.009}$	$0.117 \pm 2 \cdot 10^{-10}$	0.108 ± 0.001	$1.333 \pm 1 \cdot 10^{-5}$
d_3 [GeV^{-1}]	$0.299^{+0.020}_{-0.024}$	$0.275 \pm 3 \cdot 10^{-7}$	0.251 ± 0.073	$-0.944 \pm 5 \cdot 10^{-5}$
d_4 [GeV^{-1}]	$0.249^{+0.027}_{-0.033}$	$0.216 \pm 1 \cdot 10^{-9}$	0.183 ± 0.006	$-0.837 \pm 7 \cdot 10^{-6}$
D	$0.700^{+0.064}_{-0.144}$	$0.556 \pm 4 \cdot 10^{-8}$	0.589 ± 0.031	$0.654 \pm 9 \cdot 10^{-6}$
F	$0.510^{+0.060}_{-0.050}$	$0.460 \pm 3 \cdot 10^{-9}$	0.421 ± 0.030	$0.550 \pm 3 \cdot 10^{-6}$
V_P [MeV^{-1}]	-	3.9137 ± 0.0002	3.7773 ± 0.1927	3.1330 ± 0.0003
$Re(\alpha)$ (10^{-3})	-	$0.3597 \pm 1 \cdot 10^{-5}$	0.4265 ± 0.0366	$2.3448 \pm 3 \cdot 10^{-6}$
$Im(\alpha)$	-	$-0.2488 \pm 1 \cdot 10^{-10}$	$-0.2249 \pm 5 \cdot 10^{-8}$	$-0.0399 \pm 6 \cdot 10^{-10}$
$\chi^2_{\text{d.o.f.}}$	-	1.99	1.44	0.72

Table 4.1: Values of the free parameters and the corresponding $\chi^2_{\text{d.o.f.}}$ for the different fits described in the text. The subtraction constants are taken at a regularization scale $\mu = 630$ MeV and the value of the pion decay constant is $f_\pi = 93$ MeV. The error bars in the parameters of Models A,B and C are directly provided by the MINUIT minimization procedure.

Consequently, we proceed to analyze the pole content of the scattering amplitude, the results of which are given in Appendix I, Table I. The most eye-catching output is the generation of two poles ($z_1 = 1571.33 - i71.99$ MeV and $z_2 = 1707.00 - i207.92$ MeV) with energy positions that could be associated with the $\Xi(1620)$ and $\Xi(1690)$ known states, despite not falling within their nominal values (Eq. 1.1 and Eq. 1.2, respectively). However, the widths –especially of the second pole– have change

substantially, a fact that we will discuss further later on. Likewise, the pole at the lowest (highest) energy is strongly coupled to $\pi\Xi$ and $\bar{K}\Lambda$ ($K\Sigma$ and $\eta\Xi$) channels. These facts can be used as potential arguments to identify them with the $\Xi(1620)$ and $\Xi(1690)$ resonances.

To complete the study, we will analyze how the poles generated with the parametrization of Model 2 from our previous work [21] have moved to the positions found in this new scenario. We divide the difference in all the parameters between Model 2 and Model A into 10 intervals and, with each of these new parametrizations, search for potential poles. Fig. 4.2 represents this evolution, clearly showing how the pole at the lowest energy, $z_p = 1608.51 - i85$ MeV, has moved to the current position at $z_1 = 1571.33 - i71.99$ MeV. As for the pole at the highest energy, $z_p = 1686.17 - i14.86$, upon crossing the $\bar{K}^0\Sigma^0$ threshold, it becomes a virtual pole transitioning to a non-physical Riemann sheet (RS). Subsequently, it reappears on the second RS with a significantly larger width, eventually assuming the position $z_2 = 1707.00 - i207.92$ MeV. This phenomenon is due to the opening of the $\bar{K}^0\Sigma^0$ channel, which increases the decay probability and, therefore, leads to a broader width due to its strong coupling to this channel.

The Belle Collaboration modeled the signal of the resonances using a Breit-Wigner function, as shown in Fig. 3.4. However, our peaks (depicted in Appendix I, Fig. I) exhibit a distorted shape with an effective reduction in width compared to the theoretical value due to the Flatté effect [2] [39]. This well-known effect occurs when a resonance is located below a channel threshold whose coupling to this structure is strong, distorting the typical Breit-Wigner shape of a resonance. The opening of the $\bar{K}^0\Lambda$ channel near the z_1 pole results in an experimental width around 60 MeV, in agreement with the value compiled by the PDG. The same effect is observed for the z_2 pole, which exhibits a narrow width of around 40 MeV.

[2] When the invariant energy is close to the resonance mass, the amplitude is primarily determined by the inverse of the resonance width. As soon as the threshold is crossed, the new channel introduces an additional energy-dependent contribution to the amplitude, through the width which grows very rapidly with increasing energy. As a result, the amplitude decreases quickly, creating an apparent width that is smaller than the actual width at the pole.

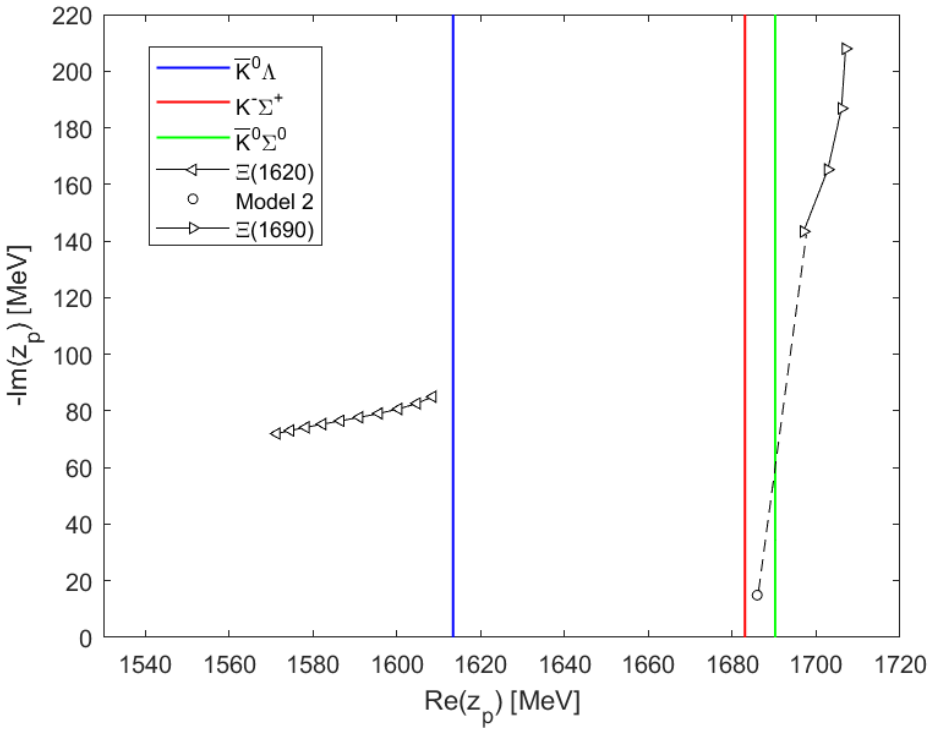

Figure 4.2: Pole positions of the $\Xi(1620)$ and $\Xi(1690)$ resonances for the approach of Model 2 in Ref. [21] and their evolution up to the parametrization of Model A of the present study.

To further explore the capabilities of the model, we can extend the ranges of the input LEC parameters up to 2σ. We perform the fit called Model B (see third column of Table 4.1) obtaining a $\chi^2_{\text{d.o.f}}$ value that is closer to the optimum, indicating a theoretical fit better matching the experimental data as shown in Appendix II, Fig. II. The new parametrization exhibits a trend where the parameters move towards the limits, following the same direction as in Model A. When analyzing the poles (Appendix II, Table II), we find that both resonances still appear with couplings that are very similar to those in Model A, but with even more pronounced shifts in their positions.

As a final test, we decided to remove the limits and perform the parametrization fit, which we will denote as Model C (fourth column of Table 4.1). It reaches the best agreement with experimental data (see Appendix III, Fig. III) and exhibits the smallest $\chi^2_{\text{d.o.f}}$ value, specifically 0.72. Also it leads to a clear improvement in the position and width of the lowest energy pole, as it can be seen in Appendix III, Table III. The

second pole is generated at slightly higher energies compared to the previous models, but with an approximately 1.5 times smaller width, closer to the PDG value. On the one hand, the fact that the $\chi^2_{\text{d.o.f}}$ is less than one indicates an (over) satisfactory theoretical fit. On the other hand, the whole our analysis also reveals a lack of sufficient data to determine our adjustable parameters in a unique and unambiguous manner.

At the moment, we shall consider Model A as our best parameter fit, because it is capable of describing the experimental Ξ_c^+ spectrum by generating the two resonances, $\Xi(1620)$ and $\Xi(1690)$, based on values of the LECs that fall within a 1σ error range from the values determined in $S = -1$ sector in Ref. [25]. This implies that we are operating within the physical validity of $SU(3)$ symmetry. Additionally, as it can be seen in Table 4.1, we observe that the minimum of Model A is very sharp, since the uncertainties for all the parameters in the model, as estimated by MINUIT, are extremely small, in contrast to, for example, Model B.

In summary, the incorporation of UχPT scheme, taking into account higher order contributions for the first time, is able to explain with sufficient accuracy the experimental evidence in the final $M_{\pi^+\Xi^-}$ spectrum and reproduce the $\Xi(1620)$ and $\Xi(1690)$ molecular states, even with only 100 experimental data points for the fitting. However, to completely determine all the model parameters we would need more experimental data in this sector. An ongoing analysis of the $K^-\Lambda$ ($S = -2$, $Q = -1$) Correlation Function using Femptoscopy Techniques by the ALICE Collaboration [40] potentially could help us to resolve this situation. This will be the next step in our research.

Chapter 5

Conclusions

The study of double strange Ξ resonances is important as their multiplicity should be on par with that of nucleon ones according to quark models. However, the current number of measured Ξ states is significantly smaller, which raises questions about their nature and internal structure.

Motivated by this fact, in previous works [20, 21] we focused on the $\Xi(1620)$ and $\Xi(1690)$ states, where the assignment of their spin-parity is incomplete. Several theoretical and experimental studies have associated them with a molecular origin of a meson-baryon system with the quantum numbers $J^P = 1/2^-$. Thus, our objective was to generate both resonances at the same time using effective field theories based on s-wave interactions between pseudoscalar mesons and octet baryons. We conducted our study within the Unitarized Chiral Perturbation Theory (UχPT) framework, incorporating not only the leading Weinberg-Tomozawa (WT) term, but also the Born terms and next-to-leading-order (NLO) contributions for the first time in this sector. Most of the model parameters were taken from the BCN model in the $S = -1$ sector [25], assuming $SU(3)$ symmetry, while the substraction constants were taken as free parameters within their natural size limits $[-3.5, -1]$. With these considerations, our model successfully dynamically generated both $\Xi(1620)$ and $\Xi(1690)$ states in a very reasonable agreement with their known positions and widths.

In recent years, heavy hadronic decays of charm baryons have emerged as a new analysis method for hadron spectroscopy. Notably, the experiment conducted by the Belle Collaboration [7] allowed the observation of signals from both $\Xi(1620)$ and $\Xi(1690)$ resonances in the final $\pi^+\Xi^-$ state through the $\Xi_c^+ \to \pi^+\pi^+\Xi^-$ weak

decay. Building upon these findings, our goal has been to extend our research by applying our theoretical model based on the chiral unitary approach to explain these experimental data.

To describe the Ξ_c^+ decay, governed by the $c \to s$ weak transition, we have used the dominant diagram (Fig. 3.1) taking into account the Cabibbo-Kobayashi-Maskawa matrix, color suppressions, diquark correlations and kinematical restrictions. This mechanism has allowed us to determine the relative fractions of the intermediate meson-baryon states formed after the hadronization process. Subsequently, these new states re-scatter through strong interactions into the final $\pi^+\Xi^-$ state, which has been parametrized by the decay amplitude $\mathcal{M}_{\pi^+\Xi^-}$, considering the UχPT scheme discussed above.

Consequently, based on our theoretical prediction of the $\pi^+\Xi^-$ mass distribution, we have been able to more precisely refit all the parameters of our model using the Belle data sample. Our best MINUIT parametrized fit, Model A with a $\chi^2_{\text{d.o.f}}$ value of 1.99, successfully reproduced the experimental data, clearly showing two peaks corresponding to the $\Xi(1620)$ and $\Xi(1690)$ resonances. With the new parametrization, we searched for poles in the second Riemann sheet of the scattering amplitude. The results revealed the presence of two poles: $z_1 = 1571.33 - i71.99$ MeV and $z_2 = 1707.00 - i207.92$ MeV, finding that the lowest (highest) energy one strongly couples to $\pi\Xi$ and $\bar{K}\Lambda$ ($K\Sigma$ and $\eta\Xi$) states. The broader width of the second pole is attributed to the opening of the $\bar{K}^0\Sigma^0$ channel, to which it couples strongly.

In our model it is possible to get even better agreement with the Belle data, reaching $\chi^2_{\text{d.o.f}}$ less than 1 (Model C). However, we consider Model A to be the best fit because it not only reasonably describes the Ξ_c^+ decay data, but also generates two poles in the scattering amplitude at reasonable positions, and maintains all the LECs close enough (within 1σ interval) to the values determined in the $S = -1$ sector, where these were fitted to a much larger amount of experimental data.

Based on the findings, the reliability of chiral models with unitarization in coupled channels has been demonstrated, highlighting the importance of considering Born and NLO contributions for precise calculations. This theoretical framework has proven

to be sufficient in accurately explaining the experimental evidence observed in the $\mathcal{M}_{\pi^+\Xi^-}$ spectrum and reproducing the $\Xi(1620)$ and $\Xi(1690)$ molecular states, despite their values falling outside the experimental compiled data in the PDG. However, it is worth noting that further improvement in the accuracy of the results could be achieved by fitting the model with additional experimental data. In this regard, the ongoing analysis of the $K^-\Lambda$ Correlation Function by the ALICE Collaboration [40] could provide a valuable opportunity for this purpose.

Appendix I: Model A

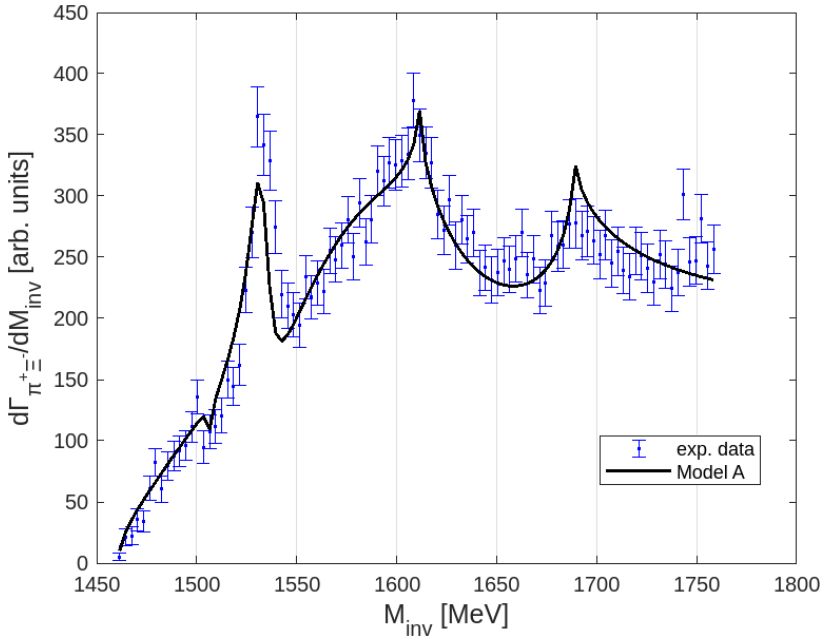

Figure I: The $\pi^+\Xi^-$ invariant mass distribution obtained with Model A (solid line) with the experimental data (points with errorbars) provided by the Belle Collaboration [38].

Model A				
M [MeV]	1571.33		1707.00	
Γ [MeV]	143.97		415.84	
	g_i	$\lvert g_i\rvert$	g_i	$\lvert g_i\rvert$
$\pi^+\Xi^-$	$-1.65 - i0.75$	1.82	$-0.22 - i0.56$	0.60
$\pi^0\Xi^0$	$1.17 + i0.55$	1.29	$-0.43 + i0.24$	0.50
$\bar{K}^0\Lambda$	$1.89 + i0.23$	1.91	$-0.27 - i0.10$	0.29
$K^-\Sigma^+$	$-0.61 + i0.14$	0.62	$-0.67 - i1.52$	1.66
$\bar{K}^0\Sigma^0$	$0.02 - i0.20$	0.20	$1.30 + i1.63$	2.08
$\eta\Xi^0$	$-0.26 - i0.14$	0.29	$1.24 + i0.56$	1.36

Table I: Pole positions of Model A with their couplings g_i and the corresponding modulus found in $J^P = \frac{1}{2}^-$, $(I, S) = (\frac{1}{2}, -2)$.

Appendix II: Model B

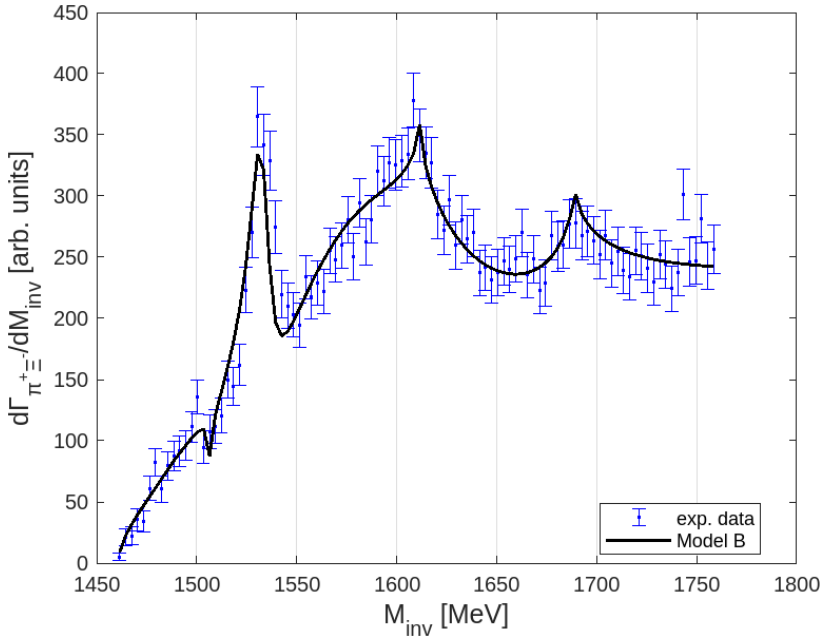

Figure II: The $\pi^+\Xi^-$ invariant mass distribution obtained with Model B (solid line) with the experimental data (points with errorbars) provided by the Belle Collaboration [38].

Model B				
M [MeV]	1564.55		1764.38	
Γ [MeV]	143.11		451.27	
	g_i	$\lvert g_i\rvert$	g_i	$\lvert g_i\rvert$
$\pi^+\Xi^-$	$-1.66 - i0.77$	1.83	$-0.22 - i0.50$	0.55
$\pi^0\Xi^0$	$1.18 + i0.57$	1.32	$-0.47 + i0.25$	0.53
$\bar{K}^0\Lambda$	$1.79 + i0.26$	1.81	$-0.23 - i0.12$	0.26
$K^-\Sigma^+$	$-0.59 + i0.10$	0.60	$-0.64 - i1.54$	1.67
$\bar{K}^0\Sigma^0$	$0.09 - i0.16$	0.19	$1.28 + i1.60$	2.05
$\eta\Xi^0$	$-0.29 - i0.16$	0.33	$1.28 + i0.47$	1.37

Table II: Pole positions of Model B with their couplings g_i and the corresponding modulus found in $J^P = \frac{1}{2}^-$, $(I, S) = (\frac{1}{2}, -2)$.

Appendix III: Model C

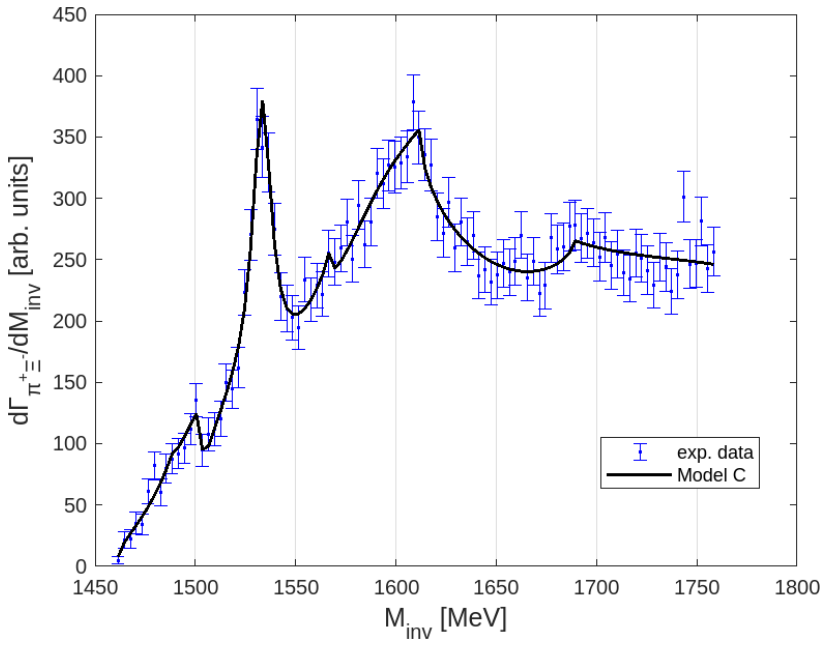

Figure III: The $\pi^+\Xi^-$ invariant mass distribution obtained with Model C (solid line) with the experimental data (points with errorbars) provided by the Belle Collaboration [38].

Model C				
M [MeV]	1574.86		1768.49	
Γ [MeV]	115.03		292.23	
	g_i	$\lvert g_i\rvert$	g_i	$\lvert g_i\rvert$
$\pi^+\Xi^-$	$-0.64 - i0.56$	0.85	$0.23 + i0.63$	0.68
$\pi^0\Xi^0$	$1.65 + i0.91$	1.89	$0.75 + i0.18$	1.96
$\bar{K}^0\Lambda$	$2.72 - i0.99$	2.89	$-0.31 + i0.18$	0.36
$K^-\Sigma^+$	$-0.66 - i0.30$	0.73	$0.30 + i0.04$	0.30
$\bar{K}^0\Sigma^0$	$-1.14 - i0.83$	1.42	$0.82 + i0.04$	0.82
$\eta\Xi^0$	$-0.44 + i0.44$	0.62	$1.60 - i0.12$	1.60

Table III: Pole positions of Model C with their couplings g_i and the corresponding modulus found in $J^P = \frac{1}{2}^-$, $(I, S) = (\frac{1}{2}, -2)$.

Bibliography

[1] S. K. Choi *et al.* (Belle Collaboration), Phys. Rev. Lett. **91**, 262001 (2003).

[2] R. Aaij *et al.* (LHCb collaboration), Phys. Rev. Lett. **115**, 072001 (2015).

[3] R.L. Workman *et al.* (Particle Data Group), Prog. Theor. Exp. Phys. **2022** Rev. Part. Phys. 2022, 083C01 (2022) and 2023 update.

[4] R. T. Ross *et al.*, Phys. Lett. B **38**, 177 (1972).

[5] A. de Bellefon *et al.*, Nuovo Cimento **28**, 289 (1975).

[6] E. Briefel *et al.*, Phys. Rev. D **16**, 2706 (1977).

[7] M. Sumihama *et al.*, Phys. Rev. Lett. **122**, 072501 (2019).

[8] C. Dionisi *et al.* (Amsterdam-CERN-Nijmegen-Oxford), Phys. Lett. B **80**, 145 (1978).

[9] S. F. Biagi *et al.*, Z. Phys. C **9**, 305 (1981).

[10] S. F. Biagi *et al.*, Z. Phys. C **34**, 15 (1987).

[11] M. I. Adamovich *et al.* (WA89 Collaboration], Eur. Phys. J. C **5**, 621 (1998).

[12] K. Abe *et al.* (Belle Collaboration), Phys. Lett. B **524**, 33 (2002).

[13] J. M. Link *et al.* (FOCUS Collaboration), Phys. Lett. B **624**, 22 (2005).

[14] B. Aubert *et al.* (BaBar Collaboration), Phys. Rev. D **78**, 034008 (2008).

[15] M. Ablikim *et al.* (BESIII Collaboration), Phys. Rev. D **92**, 092006 (2015).

[16] R. Aaij *et al.*, Sci. Bull. **66** 1278–1287 (2021).

[17] A. Ramos, E. Oset and C. Bennhold, Phys. Rev. Lett. **89**, 252001 (2002).

[18] T. Nishibuchi and T. Hyodo, EPJ Web Conf. **271** 10002 (2022).

[19] T. Sekihara, PTEP **9** 091D01 (2015).

[20] V. Valcarce, bachelor's thesis, University of Barcelona (2022).

[21] A. Feijoo, V. Valcarce and V.K. Magas, Phys. Lett. B **841**, 137927 (2023).

[22] J. A. Oller and U. G. Meissner, Phys. Lett. B **500** 263–272 (2001).

[23] A. Feijoo, V. K. Magas and A. Ramos, Phys. Rev. C **92** 015206 (2015).

[24] A. Ramos, A. Feijoo and V. K. Magas, Phys. A **954** 58-74 (2016).

[25] A. Feijoo, V.K. Magas and A. Ramos, Phys. Rev. C **99**, no. 3, 035211 (2019).

[26] A. Feijoo, PhD thesis, University of Barcelona (2017).

[27] P.G. Ratcliffe, Phys. Rev. D **59**, 014038 (1999).

[28] E. Peskin and V. Schroeder, *An introduction to Quantum Field Theory*, Westview Press (1996).

[29] B. Borasoy, R. Nißler and W. Weise, Eur. Phys. J. A **25**, 79 (2005).

[30] F.Y. Dong, B. X. Sun and J.L. Pang, Chin. Phys. C **41**, 074108 (2017).

[31] E. Oset and A. Ramos, Nucl. Phys. A **635**, 99 (1998).

[32] L.S. Geng, E. Oset and M. Doring, Eur. Phys. J. A **32**, 201–211 (2007).

[33] L. L. Chau, Phys. Rept. **95**, 1 (1983).

[34] K. Miyahara *et al.*, Phys. Rev. C **95**, 035212 (2017).

[35] W. Roberts and M. Pervin, Int. J. Mod. Phys. A **23**, 2817 (2008).

[36] A. Bramon, A. Grau and G. Pancheri, Phys. Lett. B **283**, 416 (1992).

[37] X. W. Kang, B. Kubis, C. Hanhart and U. G. Meißner, Phys. Rev. D **89**, 053015 (2014).

[38] S. Kurokawa and E. Kikutani, Nucl. Instrum. Methods Phys. Res., Sect. A **499**, 1 (2003) and other papers included in this volume; T. Abe *et al.*, Prog. Theor. Exp. Phys. 03A001 (2013) and references therein.

[39] S.M. Flatté, Phys. Lett. B **63**, 224–227 (1976).

[40] ALICE Collaboration, e-Print: 2305.19093 [nucl-ex] (2023).